Technical Assessment and Redesign of the Polaroid Captiva Film Rail Component

by

Diana Velez Garcia

B.S., Materials Science and Engineering
Massachusetts Institute of Technology, 1992

Submitted to the Department of Materials Science and Engineering and
the Alfred P. Sloan School of Management in Partial Fulfillment
of the Requirements for the Degrees of

MASTER OF SCIENCE IN MATERIALS SCIENCE AND ENGINEERING

and

MASTER OF SCIENCE IN MANAGEMENT

at the
Massachusetts Institute of Technology
May, 1994

Signature of Author _____
Department of Materials Science and Engineering and the Sloan School of Management
May 6, 1994

Certified by _____
Frederick McGarry, Professor of Polymer Engineering

Certified by _____
Karl Ulrich, Associate Professor of Management Science

Accepted by _____
Carl V. Thompson II, Professor of Electronic Materials
Chair, Departmental Committee on Graduate Students

Technical Assessment and Redesign of the Polaroid Captiva Film Rail Component

by

Diana Velez Garcia

Submitted to the Alfred P. Sloan School of Management and the Department of Materials Science and Engineering on May 6, 1994, in partial fulfullment of the requirements for the Degrees of

Master of Science in Management

and

Master of Science in Materials Science and Engineering

Abstract

The inner rail component in Polaroid Captiva integral instant film is crucial for maintaining the desired gap between the negative and positive sheets, containing the reagent liquid inside the film packet and maintaining the structural integrity of the film when it is forced through a 0.5" radius chute after a picture is taken. A technical assessment of the current seven layer laminate rail structure was undertaken for the identification of sources of material and process variability. Based on the technical assessment a novel three layer rail based on a polymer blend material was developed. Production trial data of the three layer redesign are documented and indicate significantly improved performance over the standard seven layer rail. The performance improvements of the redesign can be translated into several million dollars in annual savings. A characterization of the polymer blend material is also presented to serve as an information base for the development of relevant supplier specifications.

Thesis Advisors:

Frederick J. McGarry, Professor of Polymer Science

Karl Ulrich, Associate Professor of Management Science

Acknowledgements

My thanks go to the members of Polaroid's Materials Laboratory for their hospitality and assistance during my thesis internship. In particular I would like to thank Bill Carnes, Tony Mangano, Ed Grant, Jack Dennis and Warren Dillman for their invaluable support.

I would like to acknowledge Saroj Roy, Ralph Burpee, Bob Murphy and other members of the Polaroid research organization for their generous input of time and significant contributions to the project. I would like to thank Harry Jen, Kathy Macchiarola, and Mary McCann for making the equipment of the Polaroid Microstructure Characterization Lab available to me and assisting me in its use.

I would also like to thank Rexham Industrial for access to its manufacturing operations and Tom Bezek and Rick Brooks for their assistance throughout the project.

At MIT, my thanks go to Maureen Fahey for help with the single fiber tester, Lee Rockford for his work on the project as a UROP, and George Margaritis, Mary Chan-Park and Ramnath Subramanian for many helpful discussions and suggestions.

I would also like to thank my advisors, Frederick McGarry from the MIT Materials Science Department and Karl Ulrich from the MIT Sloan School of Management.

Finally, I would like to gratefully acknowledge the support and resources made available to me through the Leaders for Manufacturing Program.

Table of Contents

List of Figures

1. INTRODUCTION

Along with the thermal imaging system Helios, the new Captiva instant camera is considered crucial to the future profitability of Polaroid. Captiva, an auto focus, single lens reflex instant camera, is the culmination of one of the most extensive market research and development efforts in the company's history. It is designed to appeal to current 35mm camera users by being smaller than previous instant models and incorporating many of the automated exposure and focusing features associated with cameras using conventional film.

Shortly after the Captiva camera's introduction in 1992, unexpected variability in the performance of the film side seals was encountered because of high stress levels imposed on the film inside the camera. The basic configuration of the integral film used with the Captiva camera is very similar to that used in the older Spectra line of cameras. However, there is a major difference in the stresses imposed on the two types of film during processing within the camera. Spectra film is not significantly strained as it is exposed and ejected from the camera whereas the Captiva film sees significant shear and peeling stresses as it is forced through a chute with a radius of curvature of 0.5" before it is ejected. In a small percentage of frames, the shear and peeling stresses cause a failure in the side of the film packet leading to reagent leakage.

1.1 Statement of Objectives

The ultimate goal of this work was to increase the yield and performance of Captiva film by decreasing the probability of side seal leakage that takes place after the film is forced through the chute in the camera. The work focused on increasing the energy

absorption capabilities of the rail component to increase the overall performance of the side seal in the product's operating temperature range.

This thesis can be viewed as part of a three faceted effort to improve the performance of the Captiva film side seal. Parallel to the rail improvement efforts, other Polaroid groups have focused on making mechanical design changes to the camera chute configuration to reduce the stresses imposed on the film during deformation and changes to the positive and negative sheets to improve their mechanical performance without sacrificing photographic performance.

1.2 Project Approach

The approach used to improve the performance of the Captiva rail can be broken down into four steps: 1. reevaluation of rail sub-components; 2. identification of variability; 3. optimization of existing materials and 4. investigation of new material systems. The starting point of the project was a technical assessment of the current rail components. The sub-components of each layer in the rail structure were identified and evaluated for their contributions to the mechanical and adhesive properties of the rail. Next, the major sources of material variability were identified.

An optimization of existing rail materials was not undertaken because it was concluded that the current seven layer rail structure was intrinsically non-robust from a manufacturing stand-point and significant performance gains could not easily be achieved through a strategy of incremental improvement of the existing rail design. Instead, the project was redirected toward investigating new material systems which would more adequately fulfill the Captiva film product requirements. A new rail redesign which

incorporates less intrinsic material variability and is able to withstand higher stress levels during processing, thereby improving overall film yield, was developed.

1.3 Financial Impact

Production trial data of the three layer rail redesign are documented and indicate significantly improved performance over the standard seven layer rail. The performance improvements of the redesign can be translated into several million dollars in annual savings. The several million dollar estimate was calculated by considering the cost of scrap and incremental labor attributed only to the side seal leakage defect. The incremental labor figure consists of additional sampling/auditing, warehouse/inventory handling, and technician costs. The calculations used to determine the annual savings value, presented in Fig. 1.2, are stated only in general terms for proprietary reasons.

(annual production)	x (% yield loss due to side seal leakage) =	# of unshippable packs per year	
(# of unshippable packs per year not used for camera testing)	x (manufacturing and material cost per pack) =	material and production cost of defective packs	
material and production cost of defective packs	+ incremental labor cost attributed to side seal leakage =	annual savings attributed to elimination of side seal defect (on the order of several million dollars)	

Fig. 1.2 General equations used in the calculation of annual savings from elimination of side seal defect.

1.4 Thesis Organization

Chapter 2 provides an overview of the basic structure of instant film and the terminology associated with it as well as a general description of the product requirements and manufacturing processes. Chapter 3 documents a technical assessment of the rail and its subcomponents performed to identify sources of material and process variability. The work in Chapter 3 serves as a basis for the redesign strategy presented in Chapter 4. Chapter 4 summarizes the guidelines developed for a redesign of the rail and a novel three layer rail structure is presented. Chapter 4 presents production trial data for the three layer redesign which indicate performance gains that would translate into several million dollars in annual savings for Captiva film production. Chapter 5 focuses on the characterization of the primary substrate material used in the most successful redesign to serve as an information base for the future development of relevant and meaningful supplier specifications for the new design. Chapter 6 offers conclusions and closing recommendations.

2. BACKGROUND

2.1 Integral Instant Film Structure

Integral instant film provides a finished print several minutes after exposure using a system that is outwardly dry. As opposed to peel-apart films, which are comprised of sheets that are separated after processing, integral films remain intact, with exposure and viewing occurring through the same surface. In general, the integral film structure consists of a sealed sandwich with the negative and positive sheets as outer layers and a pod containing reagent attached between them. During processing, the pod is ruptured and the reagent is spread as a thin layer between the two main sheets.

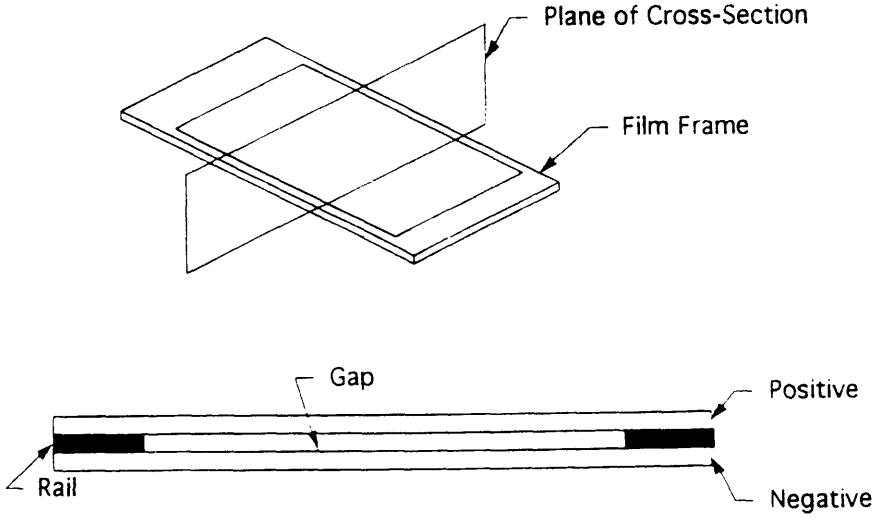

Fig.2.2 Schematic of instant film structure and cross-section

The major photographic components of instant film are the positive (also known as the sheet), the negative and the reagent. The major non-photographic components are the mask, the rails, the pod tape, the jump tape, and the trap (see Fig. 2.1). The area where the positive, rails and negative come together is referred to as the side seal (see Fig. 2.2).

The thickness of the reagent layer spread within the film is controlled by the thickness of the mask layer and the thickness of two thin material components called rails. The white mask

white mask layer, which is bonded over the clear positive sheet and frames the picture area, affects the reagent thickness by contributing to the spacing of the rollers through which the film is forced during processing within the camera (see Fig. 2.3). The thicker the mask layer, the farther apart the camera rollers are maintained, the less the picture is compressed and the larger the gap remains between the layers. The rails, which are bonded between the negative and positive sheets and along their edges also act as mechanical spacers. In addition, the rails prevent reagent leakage through the edges of the film. Once the viscosity of the reagent to be used for a run of film is characterized, the reagent gap is set by using the appropriate thickness of rail and mask.

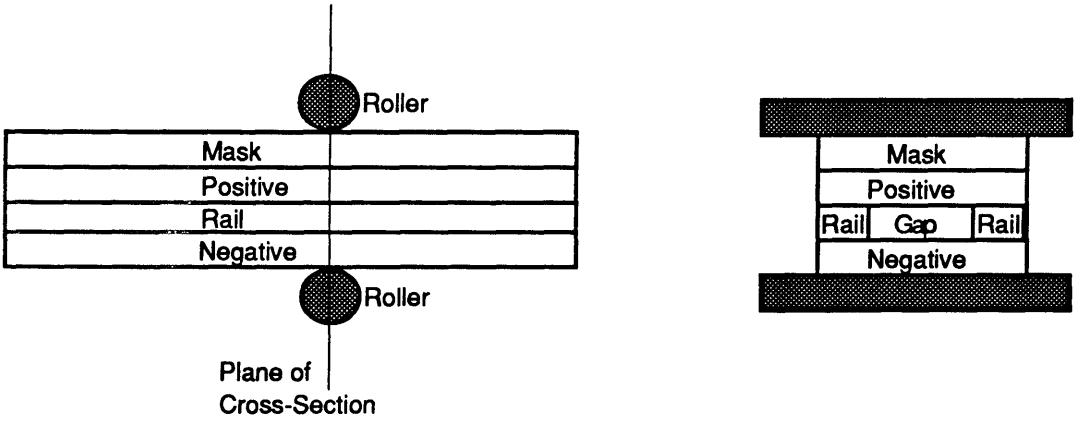

Fig. 2.3 (A) Side view schematic of film between camera rollers (B) Cross-section schematic of film between camera rollers.

2.2 Rail Structure

The rail component is a seven layer laminate structure made to total thicknesses ranging from .00217" to .00297". The rails consist of a .00142" core of white polyester sheet to which two layers of tissue paper are bonded using a polyester based laminating adhesive to which carbon black and an isocyanate cross-linking agent are added. The tissue layers range in thickness between .00025" to .00045" in .00005" increments and are used to vary the total thickness of the rail. The outer surface of each tissue layer is also coated with a layer of heat seal for adhesion either to the positive or negative sheet of

the film (see Fig. 2.4). For proprietary reasons the trade names of the rail materials are not used.

<table>
<tr><td colspan="2">POSITIVE</td></tr>
<tr><td rowspan="7">DEVELOPER</td><td>Heatseal 1</td></tr>
<tr><td>.0003" Tissue Paper</td></tr>
<tr><td>Black Laminating Adhesive</td></tr>
<tr><td>.00142" white PET</td></tr>
<tr><td>Black Laminating Adhesive</td></tr>
<tr><td>.0003" Tissue Paper</td></tr>
<tr><td>Heatseal 2</td></tr>
<tr><td colspan="2">NEGATIVE</td></tr>
</table>

Fig. 2.4 Cross-section of rail structure in film packet. Rail outlined in bold.

2.3 Film Processing Through Camera Chute

Immediately after exposure, the Captiva film is forced through a chute with a radius of approximately 0.5" (see Fig. 2.5). The positive side of the film is oriented toward the outer surface of the chute and is put in tension while the negative side is put in compression. The pod end of the film is the first to go through the chute. After traveling around the chute and before entering the transparent holding compartment the pod is ruptured and the reagent is spread between two rollers.

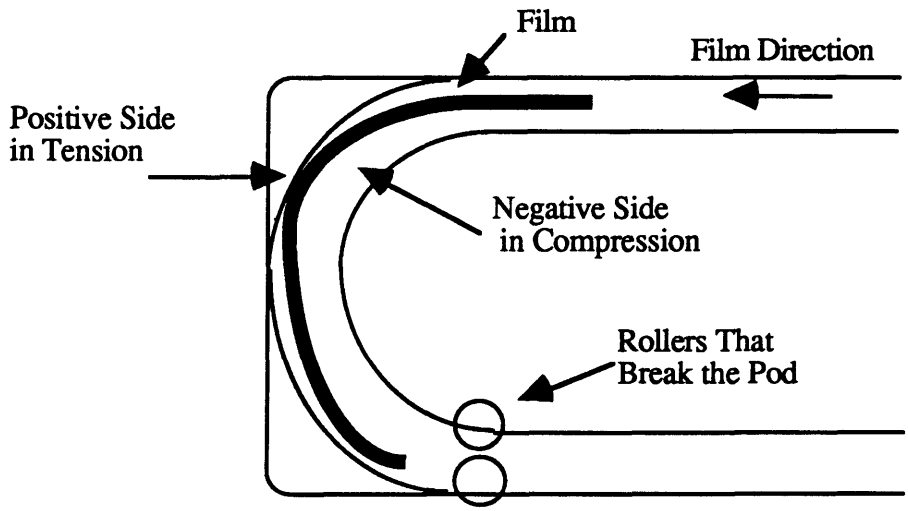

Fig. 2.5 Film path through chute.

The rail is subjected to both shear and peeling stresses as it is forced through the chute. The positive sheet is deformed to a slightly larger radius than the negative and the mismatch imposes a shear force on the rail which is sandwiched in between (see Fig. 2.6). The peeling stresses are imposed by a wave that builds up and propagates from the pod end to the trap end where it reaches its maximum. The peeling stresses do not occur normal to the edge of the film. Most of the failures in the side seal occur near the trap end where the wave reaches its maximum amplitude.

It is interesting to note that there is a propensity for failure to occur in the frames which are the first ones to be used from the frame pack. The geometry that the frames are stressed to during storage in the film cartridge depends on their position from the top. The film cartridge that holds the unexposed film frames in the camera is not symmetrical in geometry. It is skewed to one side so that the top frames are held horizontally while the bottom frames are held with a curve to one side. It follows intuition that the bottom frames are prestrained to a slight curvature and therefore are not as severely stressed

when they are forced through the chute whereas the top frames remain straight and do not have any curvature fixed into them and fail because they undergo more stress in the chute.

2.4 Rail Manufacturing Process

The rail material is manufactured by Rexham Industrial Corp. in North Carolina. The assembly of the rail laminate occurs in three passes (see Fig.2.7). During the first pass, the thinnest tissue side of the structure is laminated to the polyester core with the black adhesive. The thin side of the tissue will ultimately be oriented toward the negative side of the system.

During the second pass, the second tissue layer is laminated to the other side of the polyester sheet, with the laminating adhesive. Next there is a five day cure time to allow sufficient cross-linking in the polyester based adhesive to occur. This preliminary cure time was established empirically. After the five day cure time the material goes directly to a Gravure machine where the Heat Seal 1 is applied to the thin tissue side and Heat Seal 2 is applied to the thick tissue side.

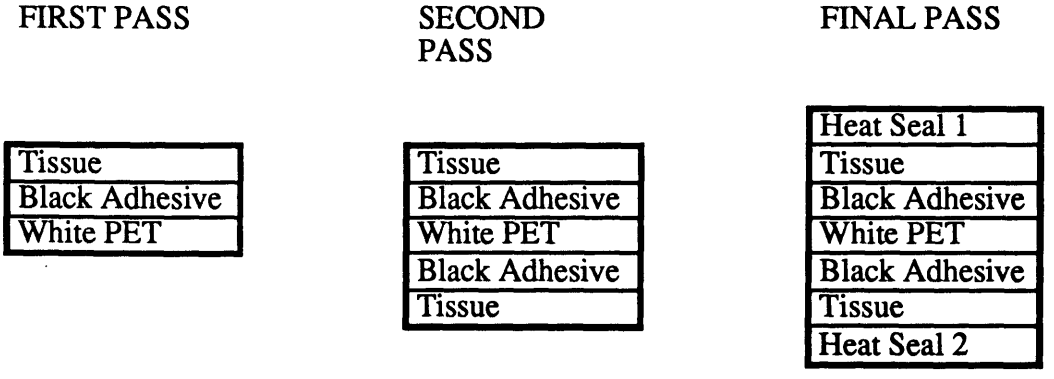

Fig.2.7 The Rail Manufacturing Process

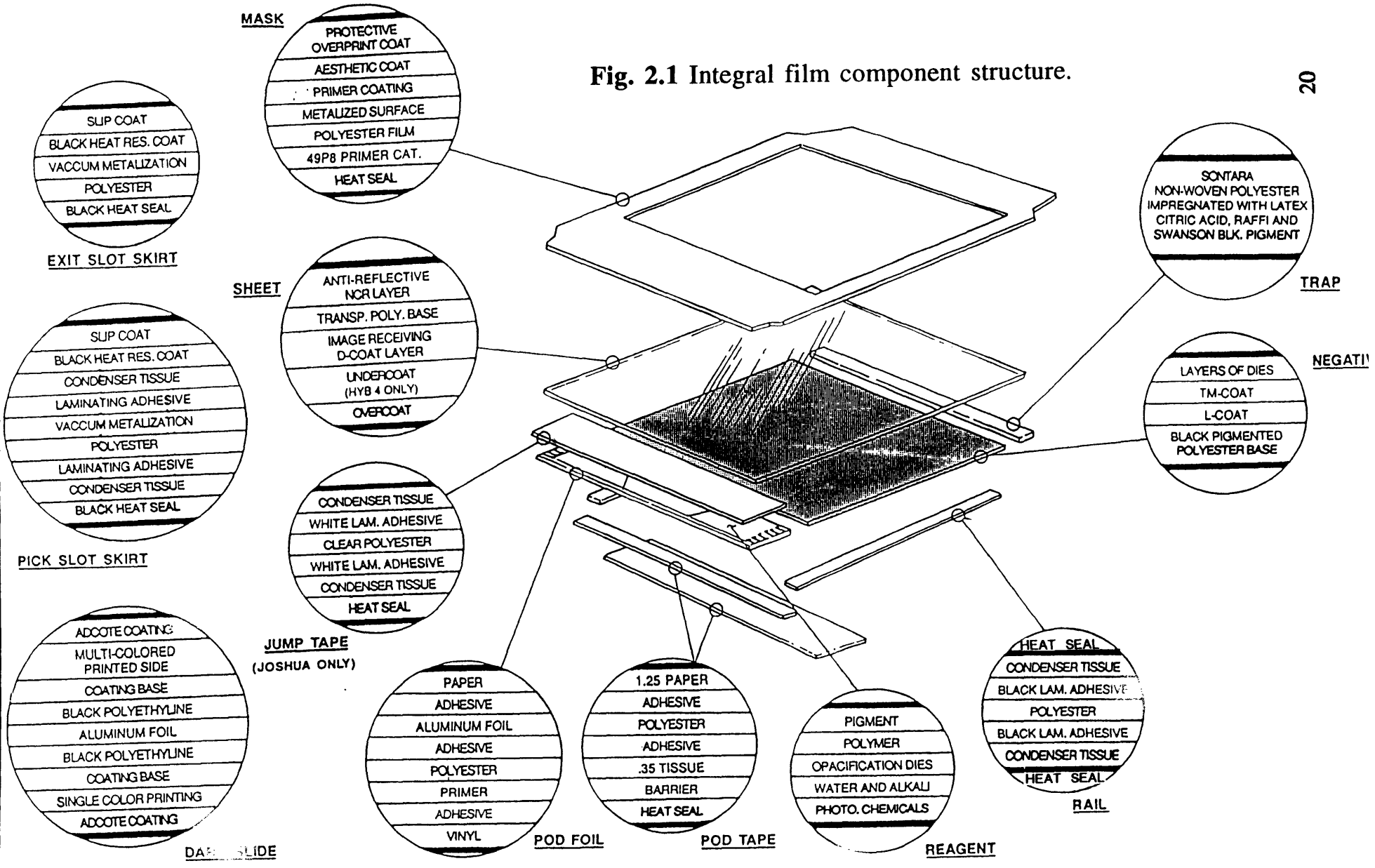

Fig. 2.1 Integral film component structure.

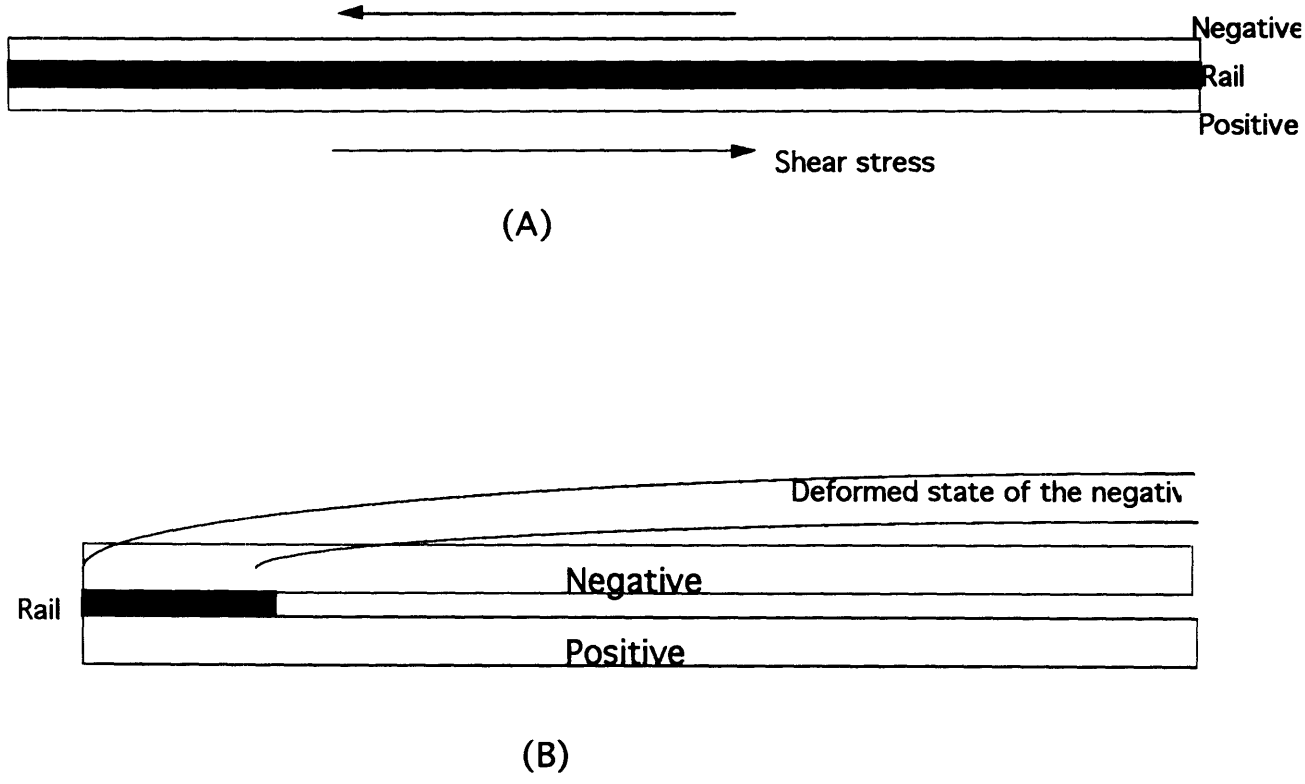

Fig. 2.6 (A) Schematic of the side view of a Captiva frame. As the frame is forced through the camera chute, shear stresses are imposed on the rail. (B) Schematic of a partial cross section of the film. The negative is shown in its unstrained as well as a deformed state. As a buckle in the negative propagates down the length of the film, peeling stresses are imposed on the rail.

3. TECHNICAL ASSESSMENT OF THE RAIL

A technical assessment of the standard seven layer laminate rail structure was conducted to gain a fundamental understanding of the failure mechanisms and sources of material and process variability contributing to the final performance of the side seal.

A characterization of the rail component's internal appearance using scanning electron microscopy was the starting point for investigating material and process variability. Rail samples, from lots representative of the extremes of rail quality as established by assembled film leakage levels, were examined in cross-section after surface cutting with a microtome to produce a smooth surface. The sample size that the micrographs represented was small, .5" samples were taken from initial rail web widths of 39" and web lengths of 5,000 to 10,000 feet. Therefore, the micrographs were not used to quantitatively characterize the rail lots but rather were used as an aid to determine areas for investigation that would lead to the reduction of material variability.

3.1 SEM Sample Preparation

A .5" x .4" piece of rail material to be studied was put between two pieces of clear plastic of the same size for structural support during cutting. The plastic and rail sandwich was then put into a sample vice holder and mounted in a Sorvall MT-2 Porter-Blum microtome. At a speed setting of .63 the surface was cut with a glass blade in ~30 micron steps until the excess plastic was cut off. Once the face was roughly even, a fresh glass knife was inserted and the cutting proceeded in 3 micron steps. The final cuts were done in 1 micron increments. The quality of the glass blades and the depth of the cuts largely determined the final quality of the surface. The quality of the cut could be

determined by the amount of distortion in the plastic. Smearing, streaking, rippling or opaqueness of the plastic material indicated a poor cut. If the surface of the material did not show any streaks and was smooth with a generally uniform thickness overall the cut was considered acceptable. At least three fresh glass knives were used in preparing each sample. After microtoming, the rail samples were coated with gold and palladium.

3.2 Microscope Settings

An accelerating voltage of 2 kV was found to be optimal for detailed micrographs of the rail cross-sections. Higher voltages resulted in unclear and uninformative micrographs. The probe current setting was 5. A Joel JSM-6300F Field Emission Scanning Electron microscope was used. The sample preparation procedure and microscope settings were determined by Ralph Burpee.

3.3 Baseline Appearance of Rail

After the examination of multiple samples, a model of the expected appearance of the rails in cross-section was developed as a baseline of information from which to identify material defects and variation.

The rail micrographs indicated a polyester core layer that was consistently uniform in thickness (see Fig. 3.1). The polyester core had a grainy surface texture with small pores. The laminating adhesive layers and the heat seal layers were characterized by smooth surfaces but varied more widely in thickness than the polyester layer. In the majority of the samples the tissue seemed to be porous. However, the porosity of the tissue layers varied between lots. It ranged from porous to dense (see Fig. 3.2). The thickness of the tissue also varied, in some areas by 2 times the specified thickness. There where also discontinuities in the tissue layer were the laminating adhesive came in contact with the heat seal layers. The variation of the tissue layer was considered to be intrinsic to the

paper material and the paper making process and was considered to be characteristic of all rail lots.

3.4 Variability Identified in Micrographs

The microscopy work done on the rail material indicated variation in the adhesive layer between the polyester core and the tissue layers. In the majority of the rail material the layer appeared uniform. However, in several lots the layer appeared cracked (see Fig. 3.3-3.4). Even though there is a possibility that the cracks were caused by the cutting action of the microtome, the cracking seems to indicate a real difference between lots of material because cracking was not apparent in all of the samples that were polished similarly.

Variability at the interfaces between layers was observed in the majority of the micrographs. Voids and areas were the laminating adhesive layer was missing were common (see Fig. 3.5). Voids in the tissue layer which caused laminating adhesive to come in contact with a heat seal layer were also observed (see Fig. 3.6).

3.5 Assembled Frames: Side Seal Cross-Sections

Fully assembled frames were also studied using the sample preparation techniques described in sections 3.1 and 3.2. Photomicrographs were taken of the frame side seals (the area where the positive, negative and rail come in contact). It was possible to identify the mask, positive, rail, negative dye, and negative base layers (see Fig. 3.7).

3.6 Assembled Frames: Deformation of Side Seal

A series of experiments was conducted in an attempt to identify the failure mechanisms of the side seal components during deformation through the camera chute. A 3/4" x 1/8" piece of frame was polished to expose the side seal cross-section. The

sample's outer non-polished edges were then dipped in fast drying epoxy and sealed. After the epoxy had dried the sample was placed in the center slit of an SEM sample holding stud into which a 5/8" diameter hole had been machined slightly off center. Using the sample holder's small side screw which is typically used only to secure the sample, the polished cross-section was forced from the side into the gap created by the drilled hole into a semi-circle. This type of deformation paralleled only the shear stresses imposed in the film during deformation in the camera, not the peeling stresses.

A series of photomicrographs were taken along the entire surface of the cross-section at four different intervals during the deformation (see Fig. 3.8 - 3.10). From this series of micrographs it is possible to observe the progression of failure in the sample. However, it is not possible to pin-point the exact defect that initiated ultimate failure which is likely to have originated deeper in the sample and not on the surface.

3.7 Assembled Frames: Peeling Stress Deformation

To study the effect that peeling stresses have on the frames, samples of side seal were prepared so that the polished surface included positive and negative sheet beyond their area of contact with the rail. The negative and positive were then forced apart using a wedge of plastic (see Fig. 3.11). Failure appeared to occur along the heat seal layer while the tissue layer appeared to remain mostly intact.

3.8 SEM Findings - Summary

The SEM micrographs provided significantly more information than the previous optical microscopy work that had been done on the structure. It was possible to

establish a baseline of information about the characteristic appearance and properties of the major rail sub-components. This work led to several preliminary findings:

1. Cracks in the adhesive layer, between the tissue and polyester, are roughly correlated with poor side seal performance.

2. The interfaces between layers are highly variable. Different levels of voids and non-uniformities were observed.

3. The tissue layer is highly variable in thickness, uniformity, adhesive penetration and density.

3.9 Dynamic Mechanical Analysis

The variation in appearance of the laminating adhesive layers between different lots of rail prompted an investigation of the mechanical properties of the adhesive layers in the material. Dynamic Mechanical Analysis was used to characterize the modulus of various rail components as a function of temperature.

Polymers are viscoelastic materials which have characteristics of both viscous liquids and elastic solids. Elastic materials have the capacity to store mechanical energy without dissipating any energy while viscous fluids have the capacity for dissipating energy but none for storing it. Therefore when polymeric materials are deformed part of the energy is stored as potential energy and part is dissipated as heat.

Typically, a material undergoes a several order of magnitude transition in modulus from a high level and brittle/elastic behavior at low temperatures to a low level and rubbery/viscous behavior at high temperatures. The typical behavior of modulus versus temperature for a polymeric material is shown in Fig. 3.12.

To determine the mechanical properties of a material as a function of temperature Dynamic Mechanical Analysis (DMA) was used. DMA is a vibrational method that measures the response (deformation) of a material to periodic forces.

In the case of sinusoidal excitation and response the applied force and the resulting deformation both vary sinusoidally with time. For linear viscoelastic behavior the strain will alternate sinusoidally but will be out of phase with the stress. This phase lag results from the time necessary for molecular rearrangements and is associated with relaxation phenomena.

During DMA analysis the specimen is subjected to an alternating strain and the stress is measured simultaneously. The stress and strain can be expressed as follows:

$$\sigma = \delta_\circ \sin(\omega t + \delta)$$
$$\varepsilon = \varepsilon_\circ \sin \omega t$$

where ω is angular frequency and δ is the phase angle.

Then $\sigma = \sigma_\circ \sin \omega\tau \cos\delta + \sigma_\circ \cos \omega\tau \sin\delta$. The stress can be considered to consist of two components, one in phase with the strain ($\sigma_o \cos\delta$) and the other 90° out of phase ($\sigma_o \sin\delta$). When these are divided by the strain, the modulus can be separated into an in-phase (real) and out-of-phase (imaginary) component. These relationships are

$$\sigma = \varepsilon_o E' \sin \omega t + \varepsilon_o E'' \cos \omega t \ ,$$

$$E' = \frac{\sigma_o}{\varepsilon_o} \cos\delta \qquad \text{and} \qquad E'' = \frac{\sigma_o}{\varepsilon_o} \sin\delta \ ,$$

where E' is the real part of the modulus, and E" the imaginary part. The complex representation for the modulus as shown in Fig. 3.13 can be expressed as follows:

$$\varepsilon = \varepsilon_o \exp i\omega t$$
$$\sigma = \sigma_o \exp i(\omega t + \delta) \ .$$

Then

$$\frac{\sigma}{\varepsilon} = E^* = \frac{\sigma_o}{\varepsilon_o} e^{i\delta} = \frac{\sigma_o}{\varepsilon_o}(\cos\delta + i\sin\delta)$$

$$E^* = E' + iE''$$

3.10 DMA Results

A Rheovibron DMA was used to scan samples of the two heat seals as well as the laminating adhesive from -50 C to 100 C at a frequency of 1 Hz (see Fig. 3.14 - 3.16). The optimal place for the rail component's transitions to occur would be at low temperatures outside of the product assembly and operating range. If this was the case, the mechanical behavior of the components would be rubbery and approximately stable in operating temperature changes. However, it was found that the transition from brittle to rubbery behavior in the laminating adhesives and heat seals occurred near room temperature. Therefore, it is predicted that order of magnitude changes in the modulus of the adhesives and heat seals occurs within small temperature changes in the product operating range.

In an attempt to identify other adhesives that would be more mechanically stable in the operating range of the product and would be suitable substitutes for the laminating adhesive, two urethane adhesives were analyzed. It was found that these adhesives did not have a more desirable DMA curve that the standard laminating adhesive (see Fig. 3.17 - 3.18). The glass transition temperatures of the two urethane adhesives were not farther from room temperature than the standard laminating adhesive nor were their moduli any lower in the operating temperature range.

Experiments were conducted to investigate the effects of humidity on the mechanical properties of the laminating adhesive. This was done in an attempt to determine the role

that exposure to moisture during lamination plays in determining the effective amount of cross-linking of the highly moisture sensitive catalyst that is added to the adhesive. It was thought that varying levels of catalyst in the adhesive might contribute to the sometimes cracked appearance of the layer as observed in the photomicrographs.

Different amounts of the isocyanate catalyst were exposed to 20% RH, 45% RH, 65% RH, 81% RH for time varying from one to eight hours. The catalyst material used in the experiments was acquired directly from the manufacturer. Its history of exposure to moisture was identical to that of the material received by Rexham and before use in their manufacturing process. After humidity exposure, the samples of catalyst were transferred to a dry box and mixed with a corresponding amount of polyester resin in a 0% RH environment. A one week cure at room temperature was also conducted a zero humidity. After the one week cure the adhesive samples were characterized using Dynamic Mechanical Analysis.

There was not a significant difference in the DMA profiles of the different samples nor were there any clear trends in mechanical behavior as a function of exposure to different levels of humidity (see Fig. 3.19a-d). The glass transition temperatures and rubbery and brittle moduli of the samples did not show either an increasing or decreasing trend.

3.11 Three-Point Bend Testing

Three Point bend tests were conducted on the rail material to measure force versus deflection. It was initially thought that it would be possible to detect internal failures, possibly in the tissue layer, as the load was increased giving the curves a saw toothed shape. Instead, the large part of the information that was gathered indicates that characteristically good material is less stiff than the bad material.

The apparatus that the three point bend tests were performed on was initially developed to measure the axial compressive and transverse tensile properties of single polymer fibers.[1] With the apparatus it is possible to measure the deflection of a sample caused by a load of dead weights (see Fig. 3.20). The sample sits on a stage that also acts as the two stationary points in the tests. A hooked probe attached to a gas bearing supported movable grip is used to apply a load in the center of the specimen as weights are added to the basket. The movable grip is attached to a cable which also runs over a gas bearing ending in a holder for the dead weights. For the approximation of linear behavior to hold, the deflections are kept small, on the order of 60 microns. An optical microscope was used to measure the deflections.

3.11.1 Sample Preparation

Two lots of rail were studied using the three point bending technique; lot 7084 and lot 7065. Lot 7084 was considered a very high quality lot resulting in zero side seal leakage after assembly whereas lot 7065 was considered to be of very poor quality resulting in high leakage levels after assembly. Samples of each rail were prepared to a thickness of 50 microns using a LKB Bromma 2218 microtome. The wooden end of a cotton swab was used to gather the rail slivers in a sample holder between passes of the microtome arm.

3.11.2 3PT Results

Curves documenting deflection versus load during loading and unloading are presented in figures 3.21 and 3.22. The samples of lot 7084 required a load of 600 mg. to reach a deflection of 60 microns whereas the samples of lot 7065 required a load of 750-

[1] McGarry, F.J. and J.E. Moalli. *Mechanical Behaviour of Rigid Rod Polymer Fibres: Measurement of Axial Compressive and Transverse Properties.* Polymer. Vol. 32, No. 10, 1991.

800 mg. to reach the same deflection. This data supports the hypothesis that stiff material is undesirable for the Captiva side seal application.

3.12 Crack Initiation

The force required to initiate failure due to peeling in a layer of the rail was studied. The apparatus described in section 3.10 was modified for crack force initiation measurements. The hooked probe and the stage were replaced with micro alligator clips. The fixed clip was attached to the polyester core and the movable clip was attached to the tissue layer. The edge cuts of rail were used in the experiments. In the rail manufacturing process a small width of the rail edges remain uncoated with black laminating adhesive. This provided an area of unlaminated tissue and polyester core for the attachment of the grips. Several attempts were made to peel the tissue layer away from the polyester core but in each case the tissue ripped and the attempts were unsuccessful.

3.13 Areas Targeted for Material Variability Reduction and Optimization of the Current Rail Structure

Work is currently being done to reduce material variability in the heat seal and laminating adhesive layers. An effort has been initiated with the suppliers of the heat seals to modify their products in such a way that the transition in modulus is shifted to a temperature below the operating range of the product while maintaining the required adhesive and laminating properties.

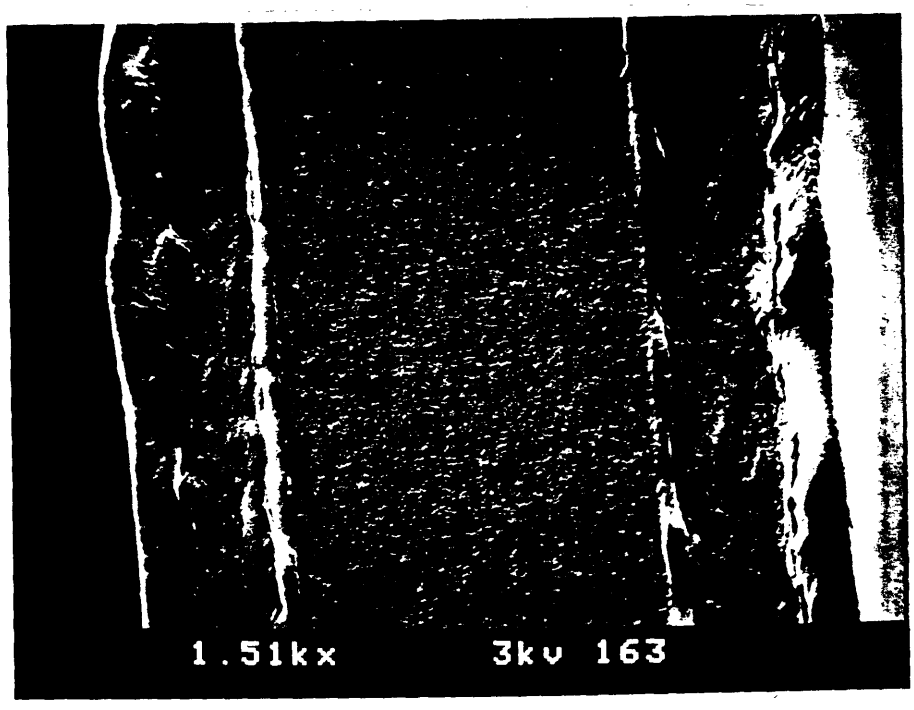

Fig. 3.1 Baseline appearance of rail. The rail is seen in cross-section at a magnification of 1,510 x.The layers are oriented vertically. From left to right, the layers apparent are: heat seal / tissue / laminating adhesive / polyester / laminating adhesive / tissue / heat seal.

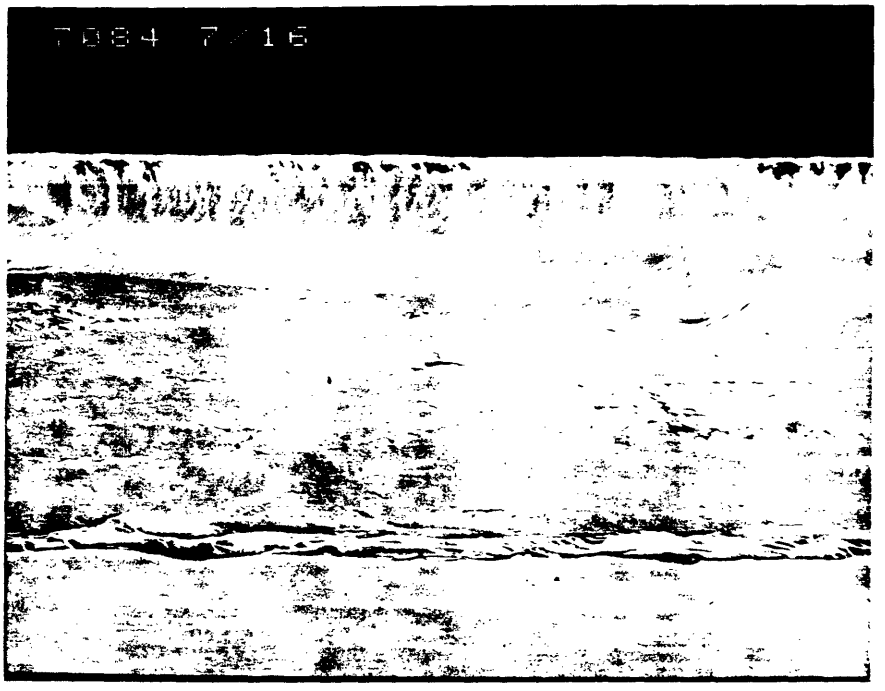

(A)

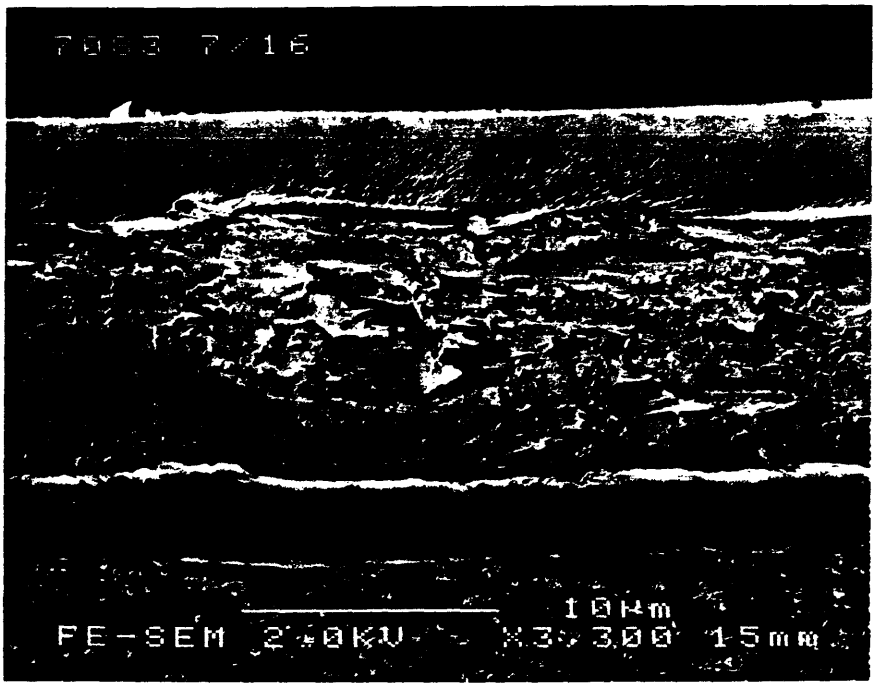

(B)

Fig. 3.2 Two micrographs are shown to contrast the different levels of porosity observed in the tissue layer. In both the micrographs the layers are oriented horizontally. Complete cross-sections are not shown. From top to bottom the layers shown are: heat seal / tissue / laminating adhesive / polyester. Only the top section of the polyester is shown. A dense tissue layer is apparent in micrograph (A) and a more porous one is apparent in (B).

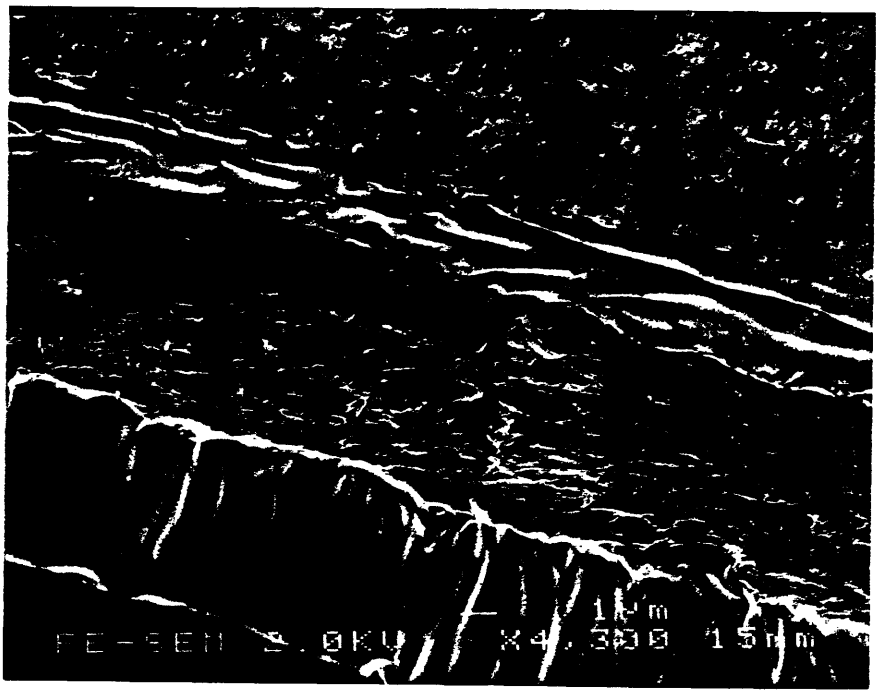

(A)

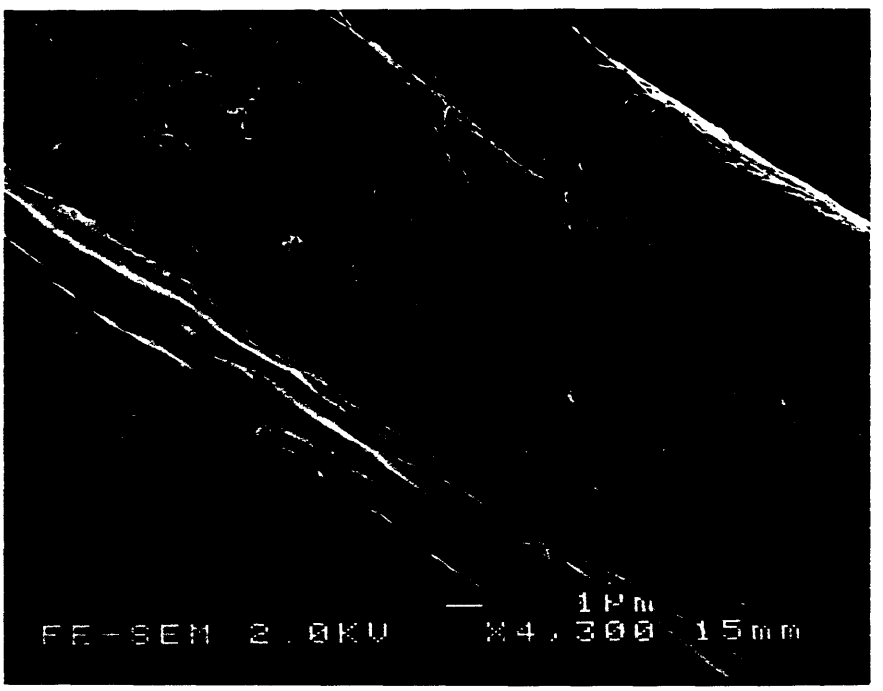

(B)

Fig. 3.3 Cracking is apparent in the laminating adhesive layers in both micrographs. (A) The rail layers from top to bottom: polyester / laminating adhesive / tissue / heat seal, are shown on a slight diagonal from the upper left corner of the picture to the lower right. (B) The rail layers from top to bottom: heat seal / tissue / laminating adhesive / polyester, are shown on a slight diagonal from the upper left hand corner to the lower right.

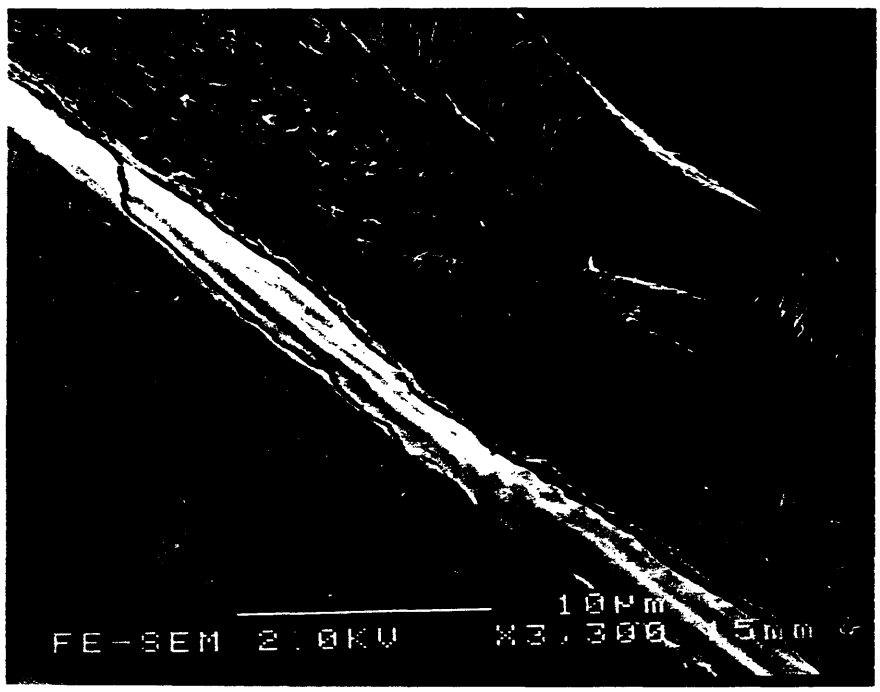

Fig. 3.4 Cracking is apparent in the laminating adhesive layer. From top to bottom the rail layers shown are: heat seal / tissue / laminating adhesive / polyester, are shown on a slight diagonal from the upper left hand corner to the lower right.

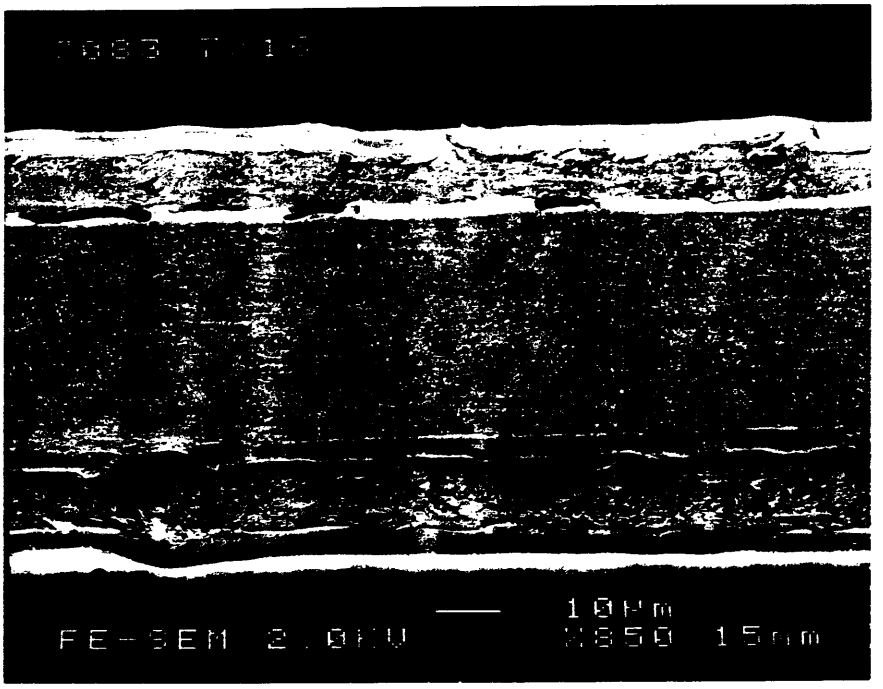

(A)

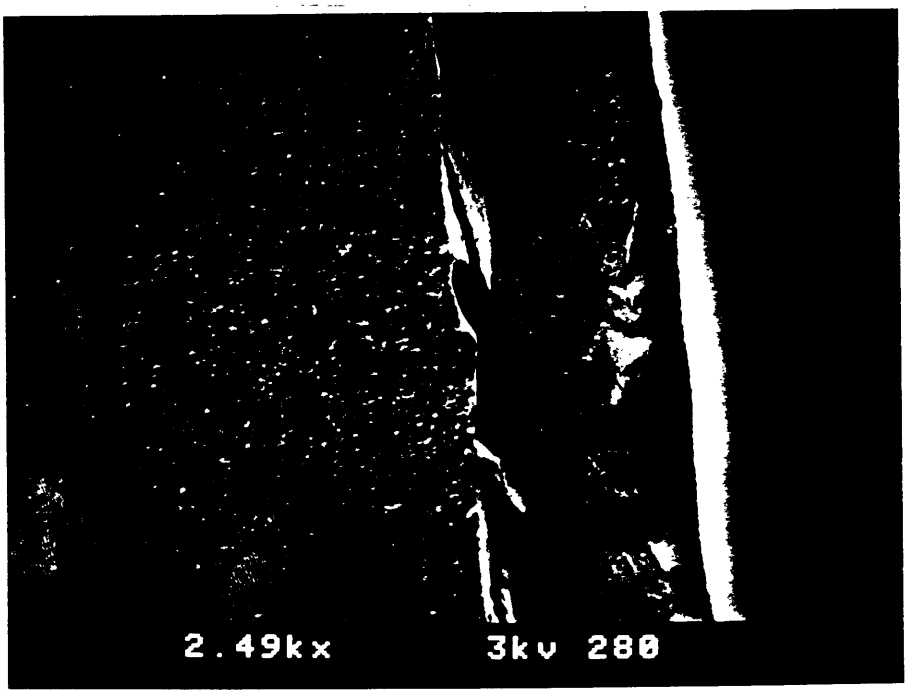

(B)

Fig. 3.5 Voids are apparent in the laminating adhesive layers in both micrographs. (A) A complete cross-section of the rail is shown with the layers oriented horizontally. (B) Only a partial cross-section of the rail is shown in a vertical orientation. From left to right the layers are: polyester / laminating adhesive / tissue / heat seal.

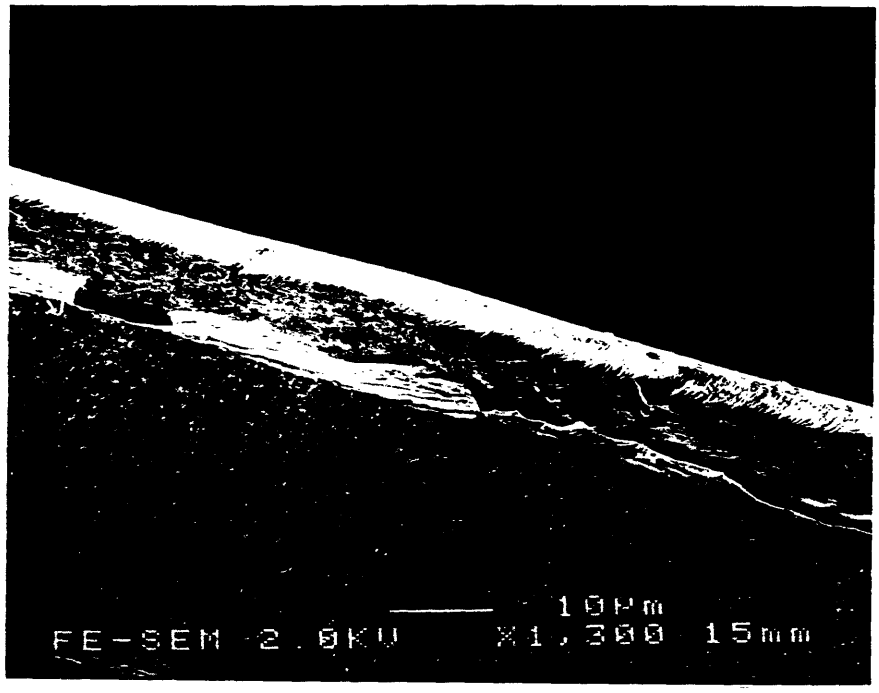

Fig. 3.5 (C) Another example of voids in the laminating adhesive layer. The horizontally oriented rail layers shown from top to bottom are: heat seal/tissue/laminating adhesive/PE

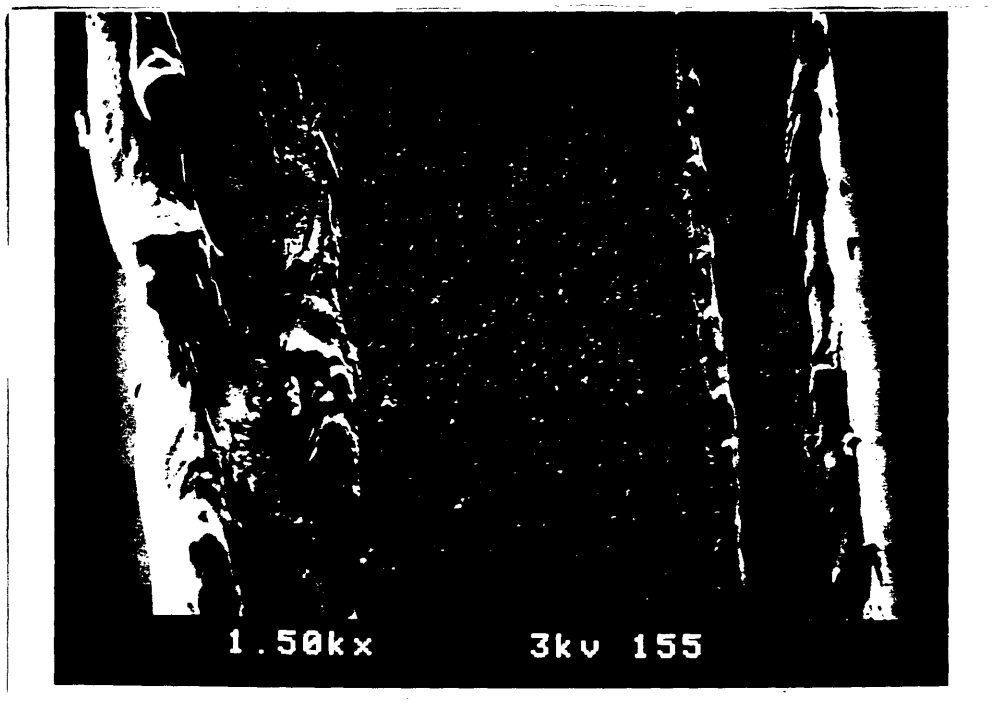

Fig. 3.6 A discontinuity in the left-most tissue layer has caused the heat seal layer to come in contact with the laminating adhesive layer. The vertically oriented rail layers, from left to right are: heat seal/tissue/laminating adhesive/polyester/laminating adhesive / tissue/heat seal.

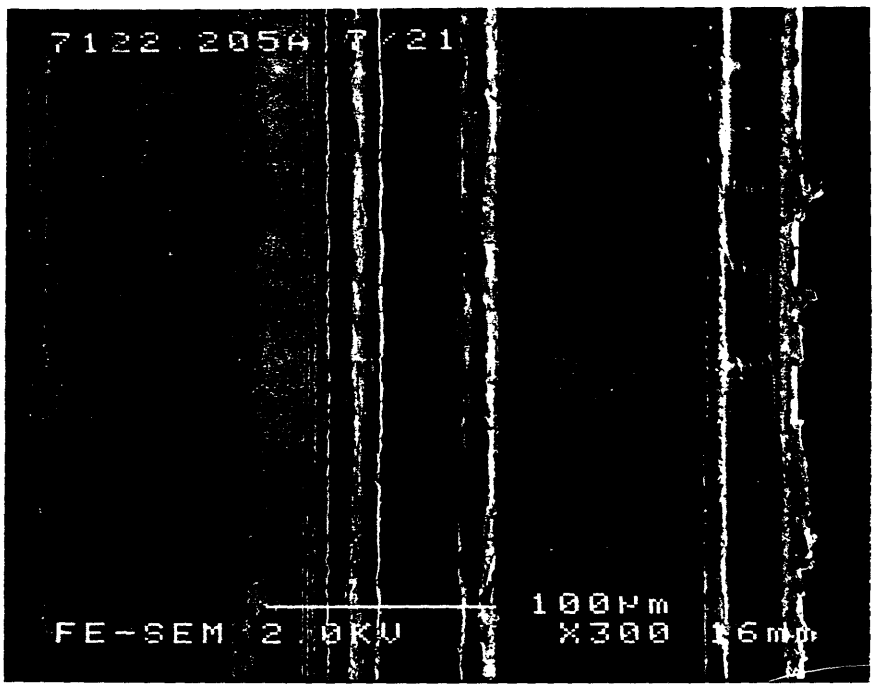

Fig. 3.7 Cross-section of the side seal of a fully assembled frame. The layers are oriented vertically beginning with the negative on the left-side. The mask, positive, rail, negative dye, and negative base layers are apparent.

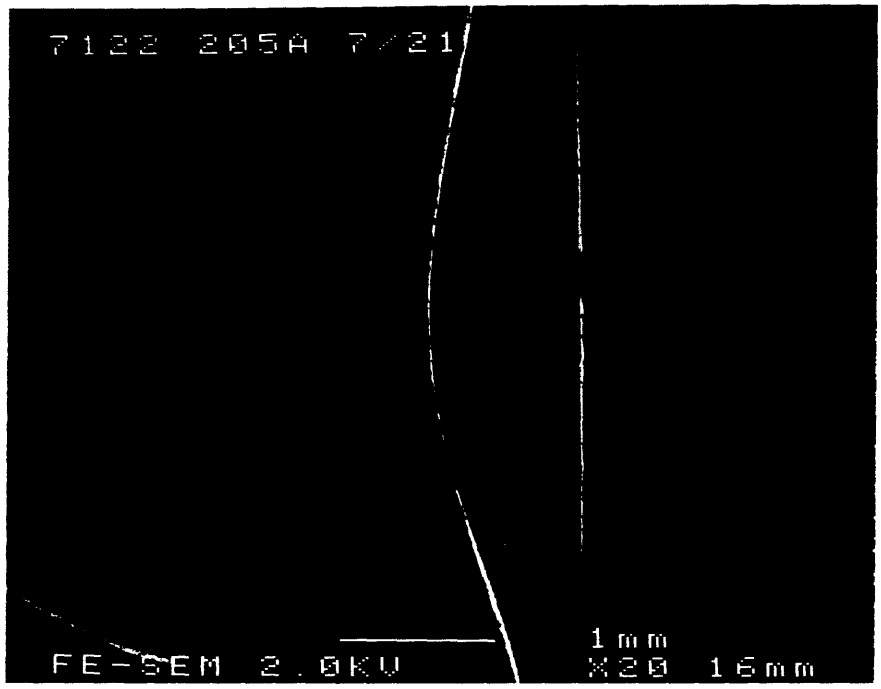

(A)

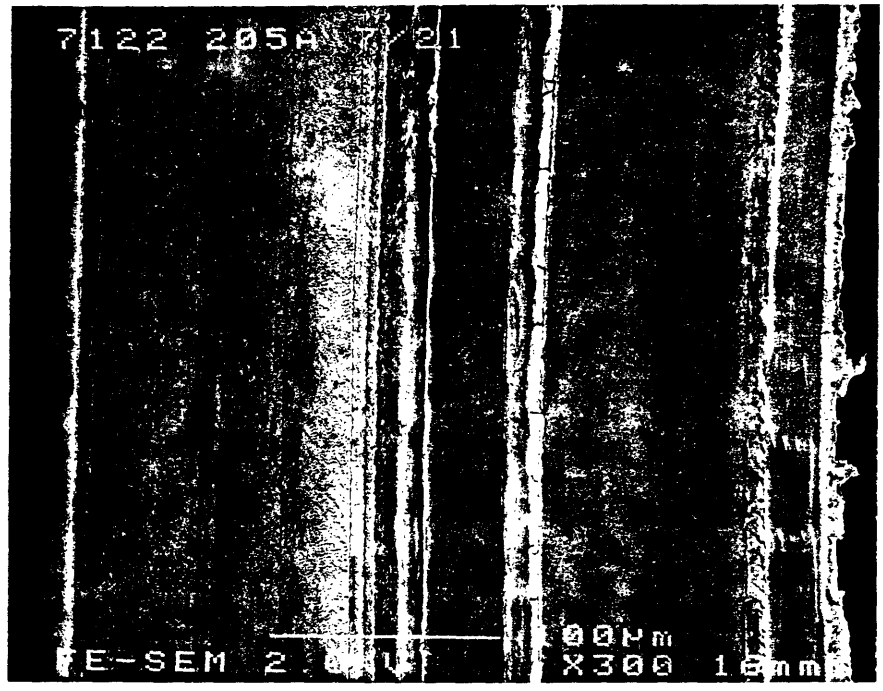

(B)

Fig. 3.8 (A) At 20x magnification, a slight curvature imposed by the sample holder is apparent in a frame side seal sample that has been polished in cross-section. (B) The same sample in micrograph (A) is shown at a magnification of 300x. Significant deformation of the side seal has not occurred

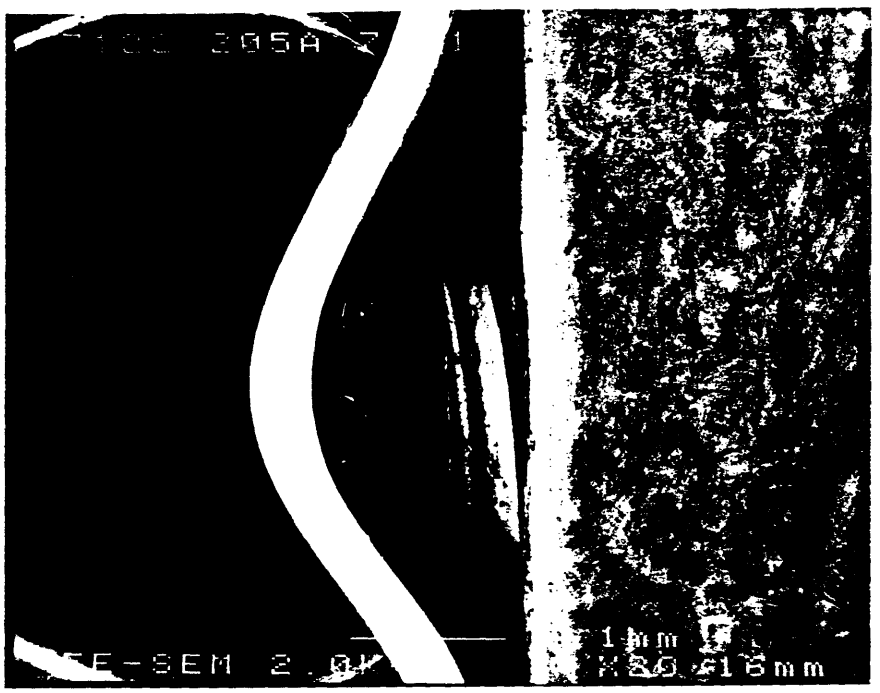

(A)

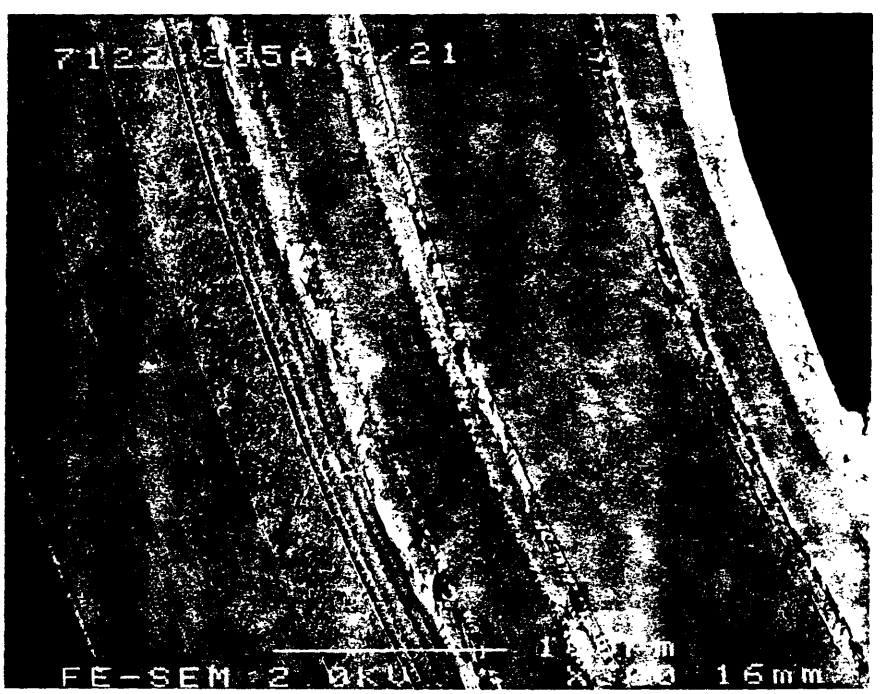

(B)

Fig. 3.9 (A) The polished frame section is shown in the modified sample holder at a magnification of 20x. The screw is shown on the right side of the sample imposing a slightly more severe curvature than is apparent in Fig. 3.8 (A).(B) The sample in (A) is shown at a magnification of 300x. Some deformation of the side seal is apparent.

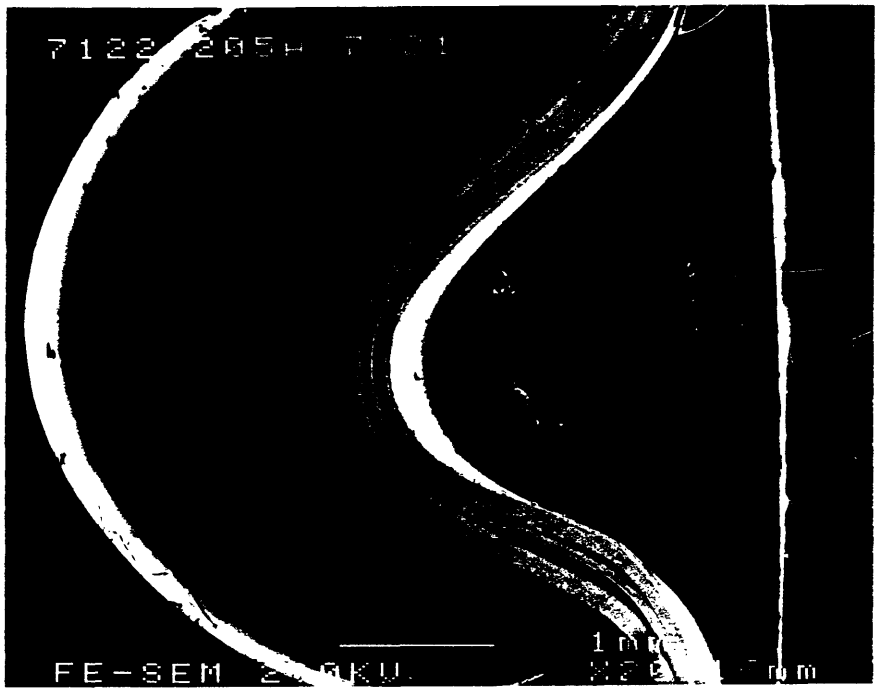

(A)

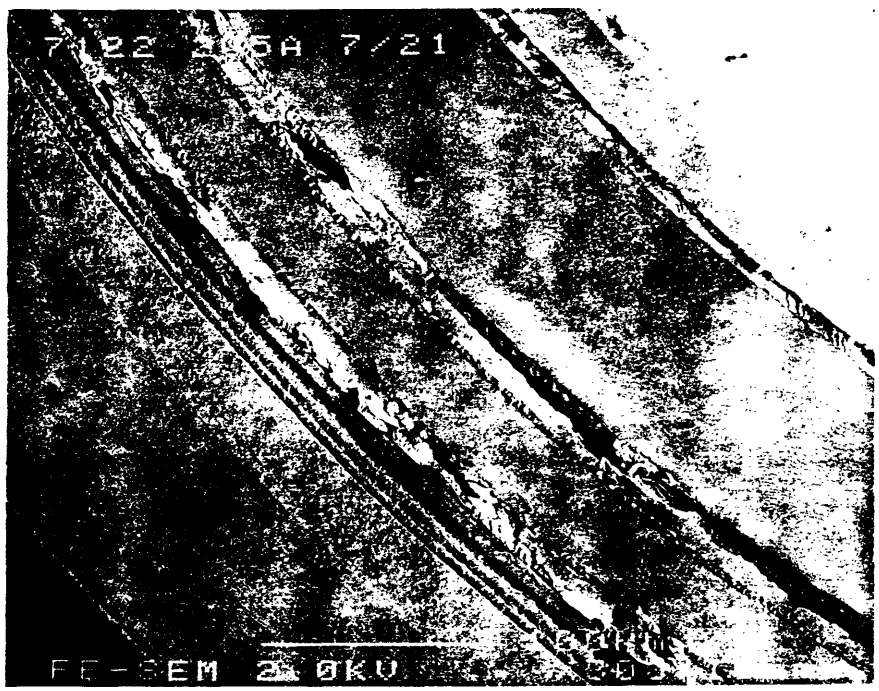

(B)

Fig. 3.10 (A) The polished frame section is shown in the modified sample holder at a magnification of 20x. The screw is shown on the right side of the sample imposing an even more severe curvature than is apparent in Fig. 3.9 (A).(B) The sample in (A) is shown at a magnification of 300x. Failure of the side seal has occurred

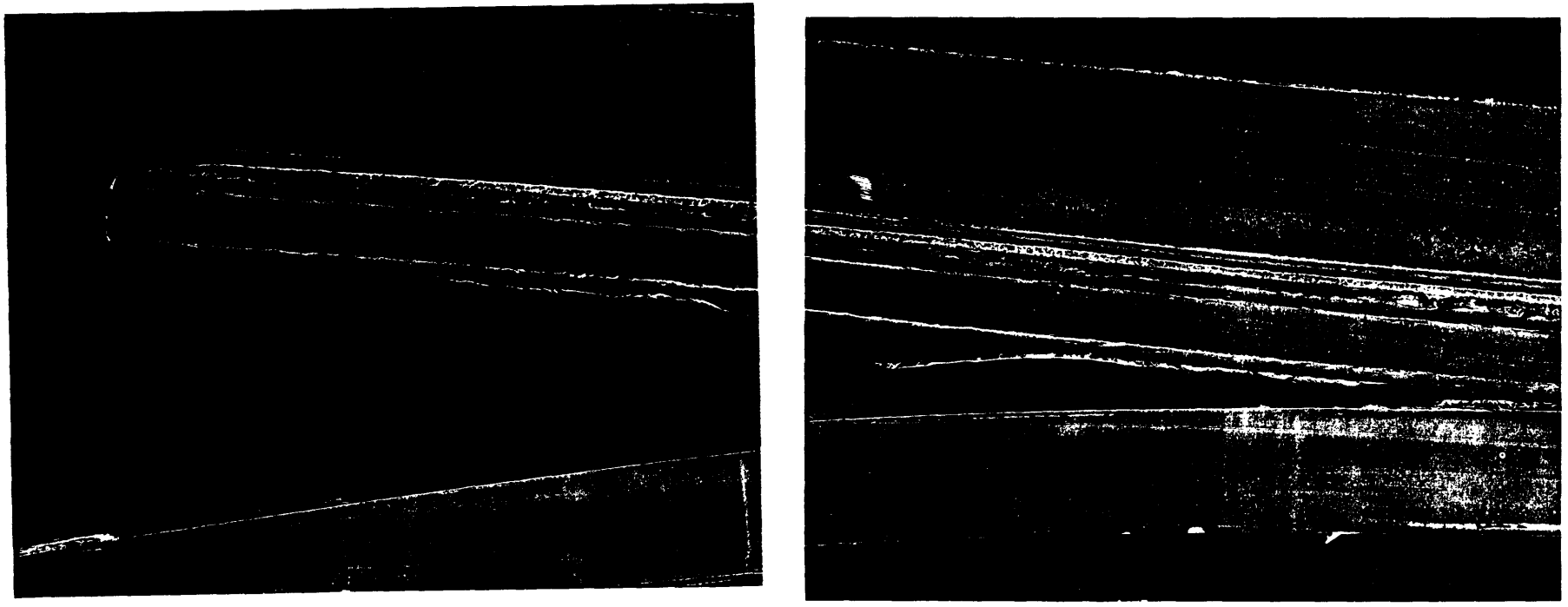

Fig. 3.11 SEM micrograph of a side seal cross-section deformed by peeling stress. The layers from top to bottom are: negative / rail / positive. The left-most end of the rail would be in contact with developer in an exposed picture. The area of the frame shown is similar to that represented schematically in Fig. 2.4. Failure occurred at the interface between the rail and the positive.

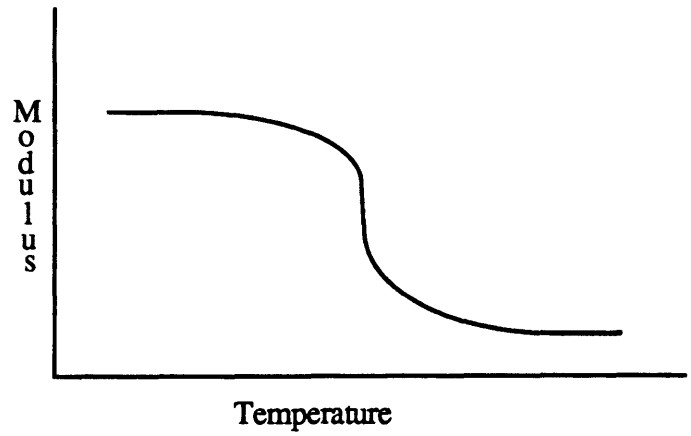

Fig. 3.12 The typical behavior of modulus versus temperature for a polymeric material.

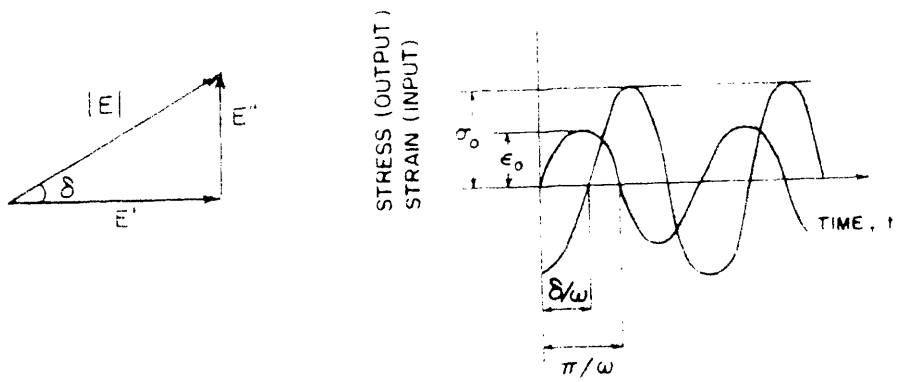

Fig. 3.13 Relations between various parameters used to express the results of a dynamic mechanical measurement.

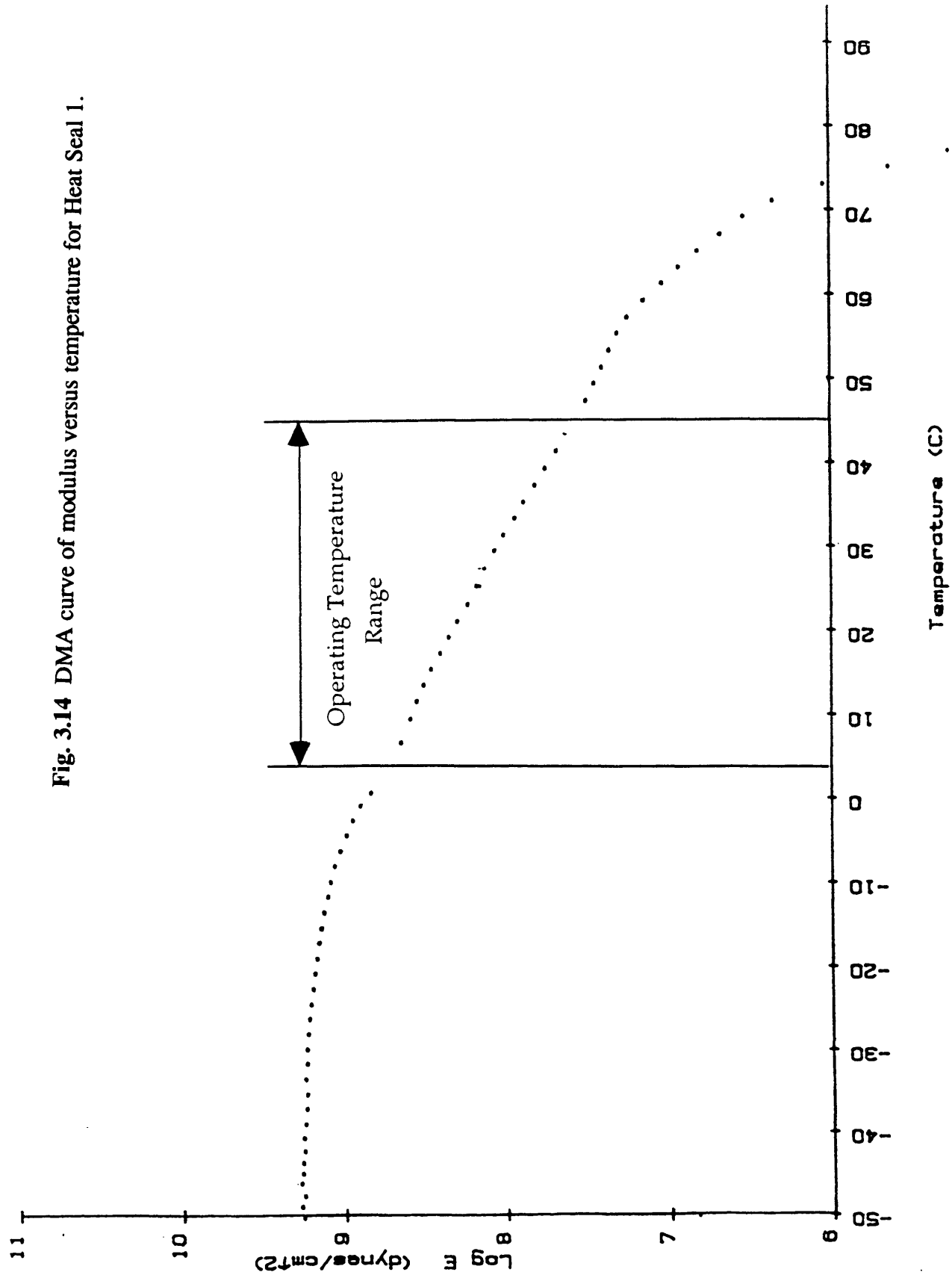

Fig. 3.14 DMA curve of modulus versus temperature for Heat Seal 1.

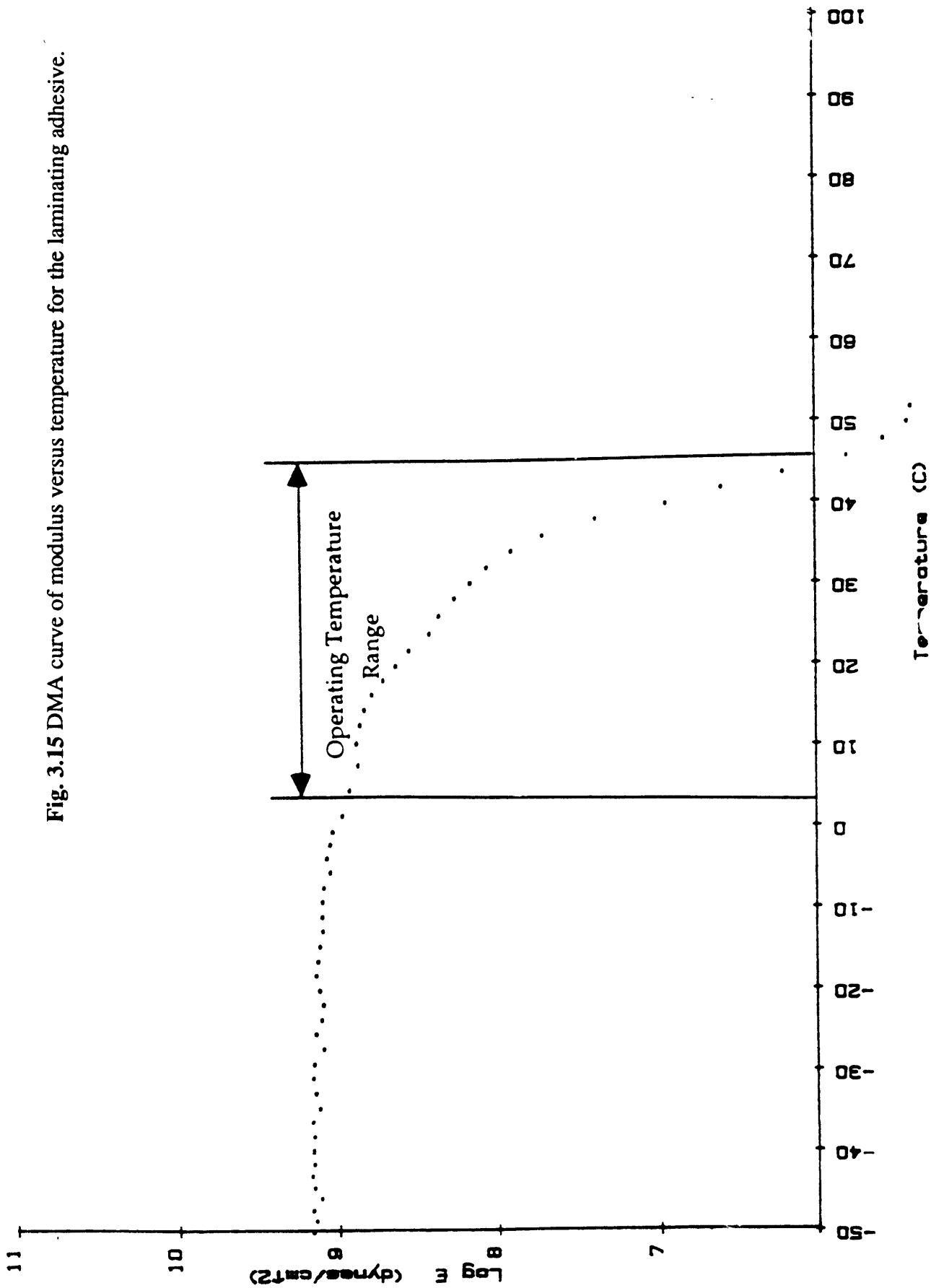

Fig. 3.15 DMA curve of modulus versus temperature for the laminating adhesive.

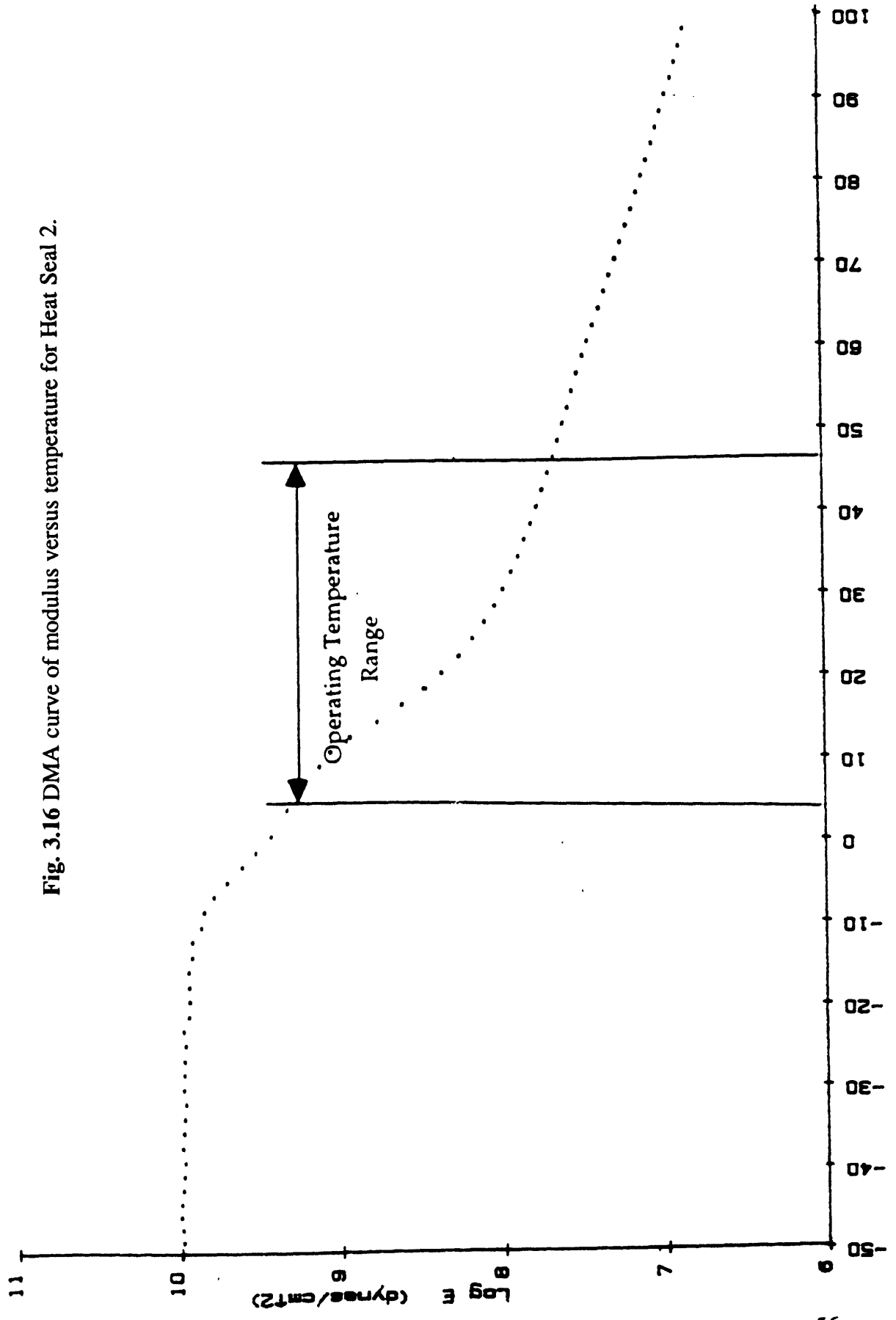

Fig. 3.16 DMA curve of modulus versus temperature for Heat Seal 2.

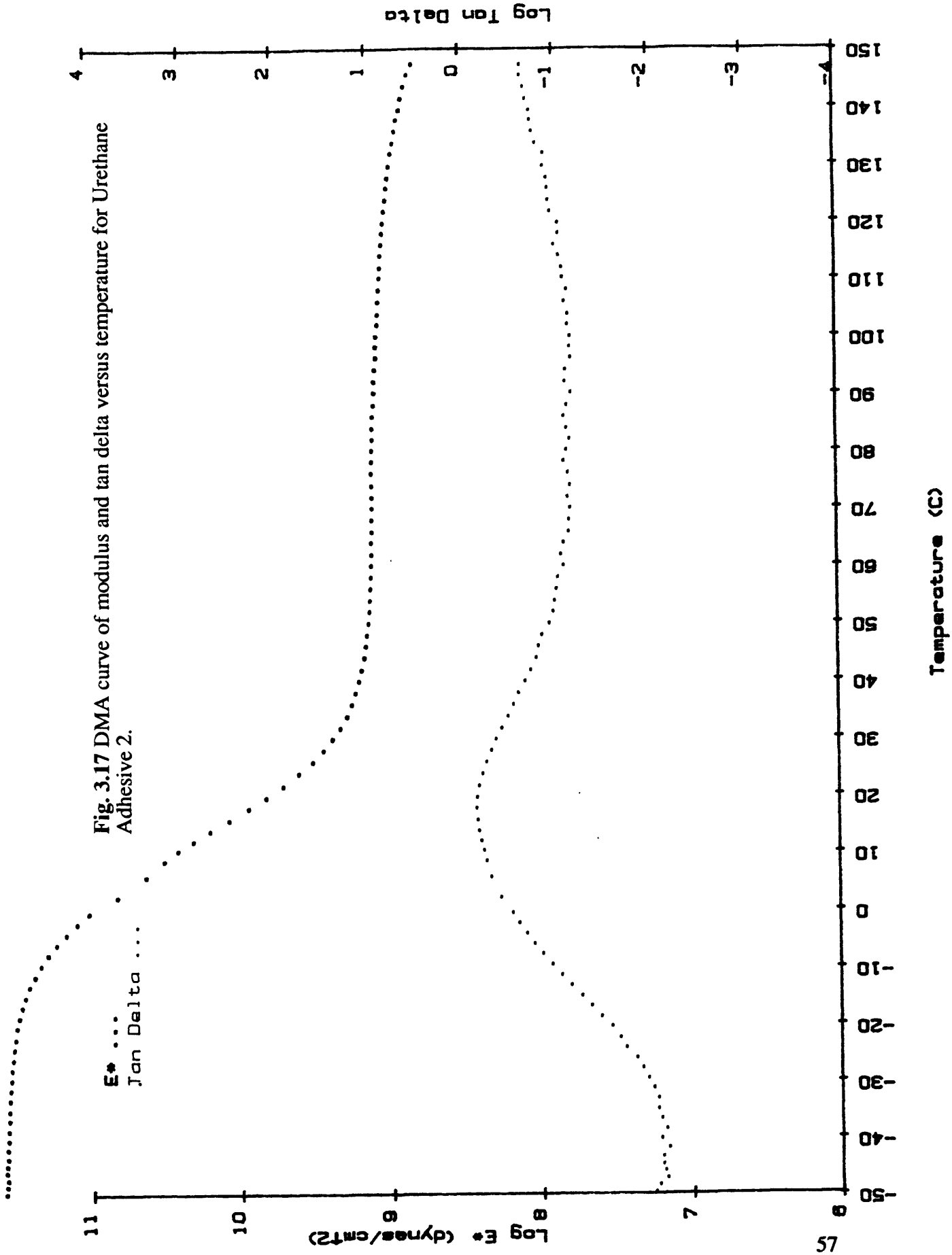

Fig. 3.17 DMA curve of modulus and tan delta versus temperature for Urethane Adhesive 2.

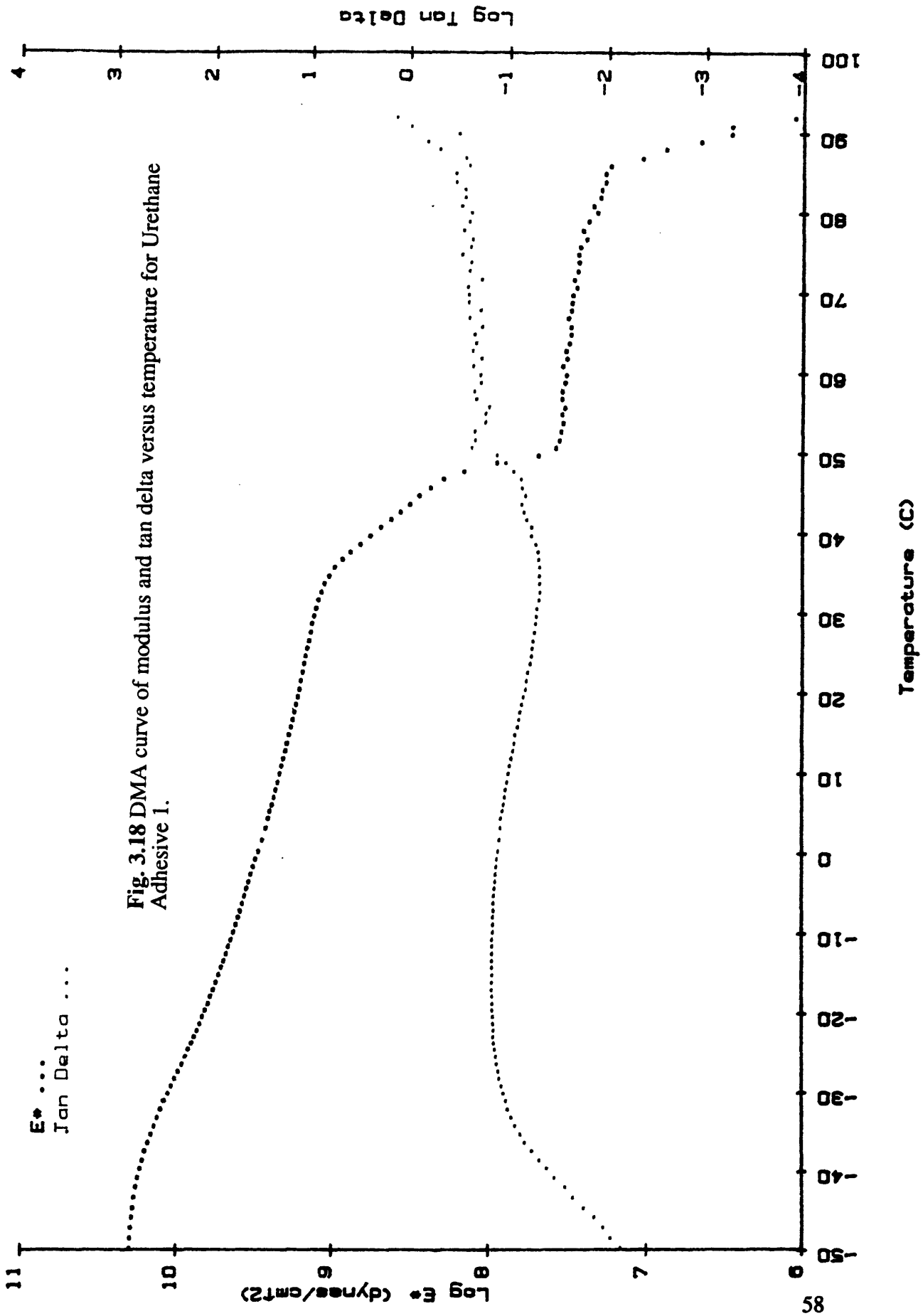

Fig. 3.18 DMA curve of modulus and tan delta versus temperature for Urethane Adhesive 1.

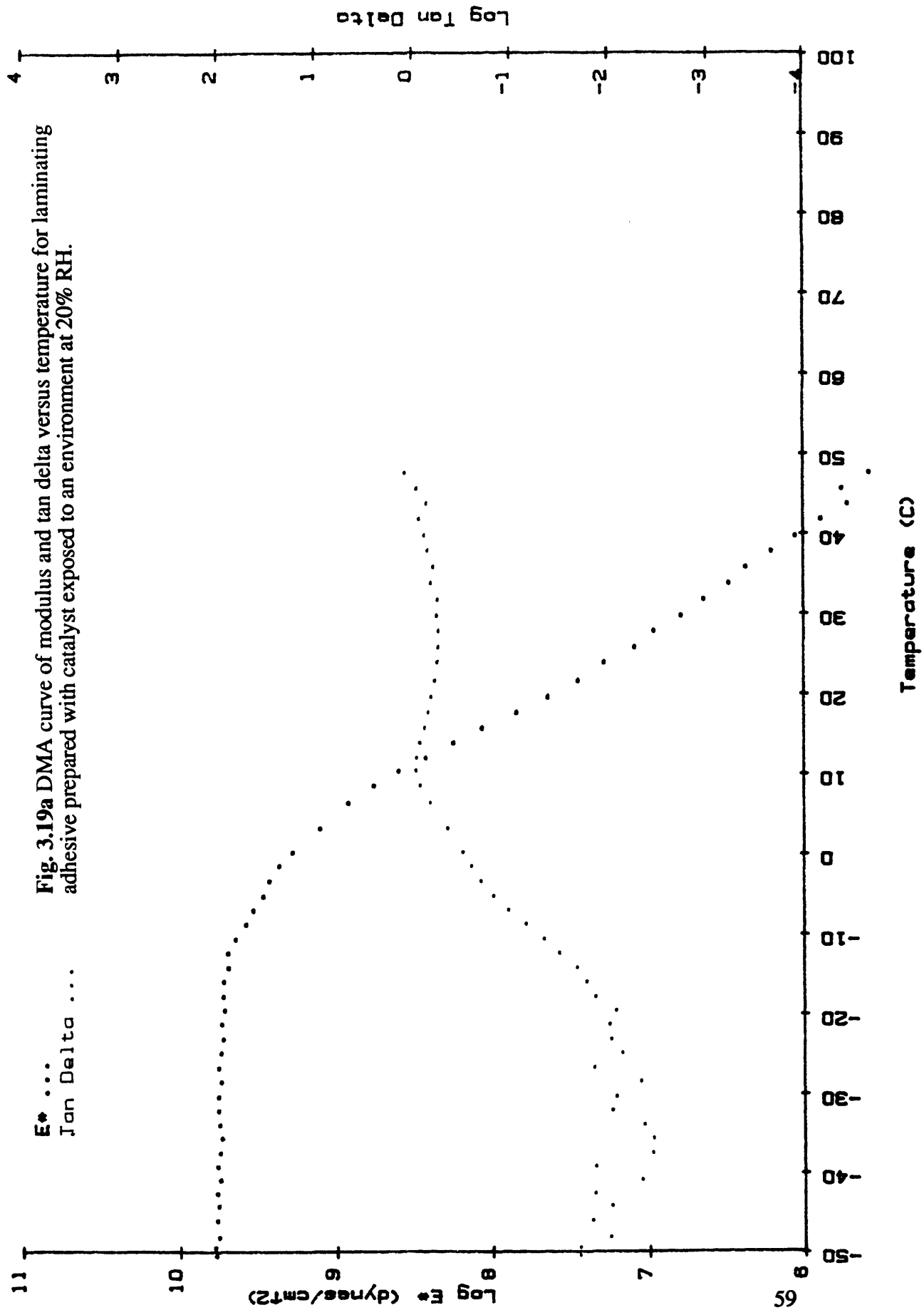

Fig. 3.19a DMA curve of modulus and tan delta versus temperature for laminating adhesive prepared with catalyst exposed to an environment at 20% RH.

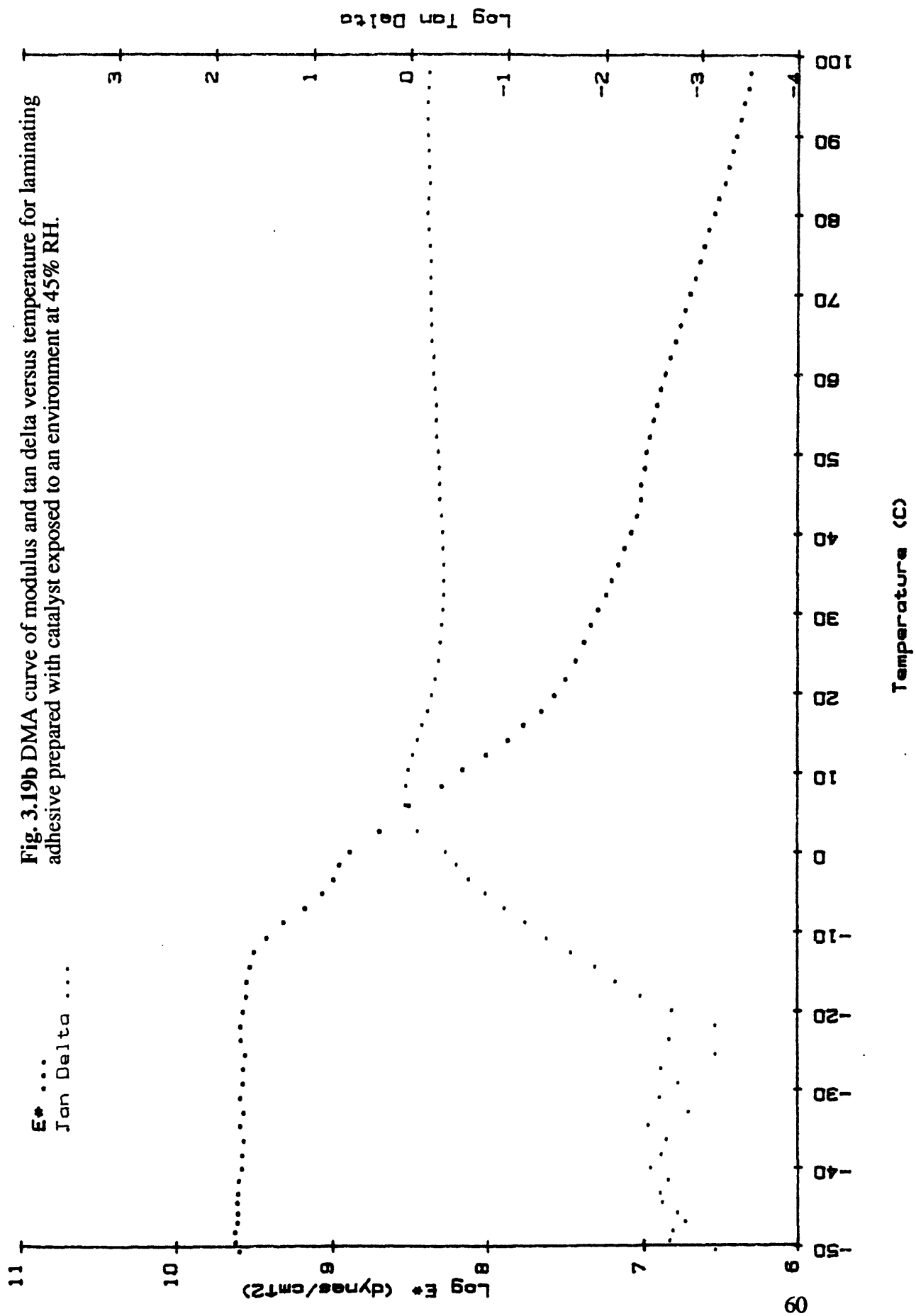

Fig. 3.19b DMA curve of modulus and tan delta versus temperature for laminating adhesive prepared with catalyst exposed to an environment at 45% RH.

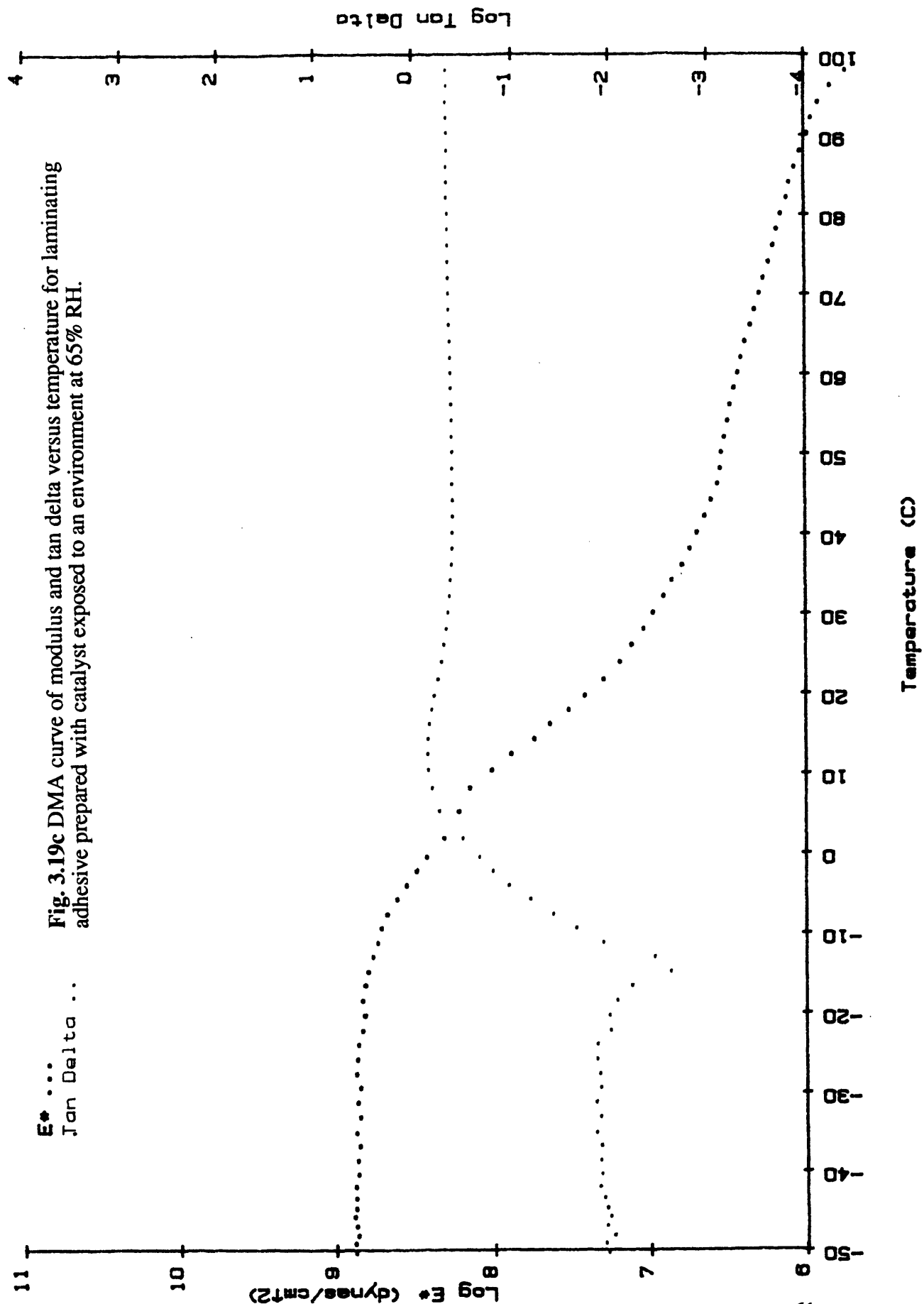

Fig. 3.19c DMA curve of modulus and tan delta versus temperature for laminating adhesive prepared with catalyst exposed to an environment at 65% RH.

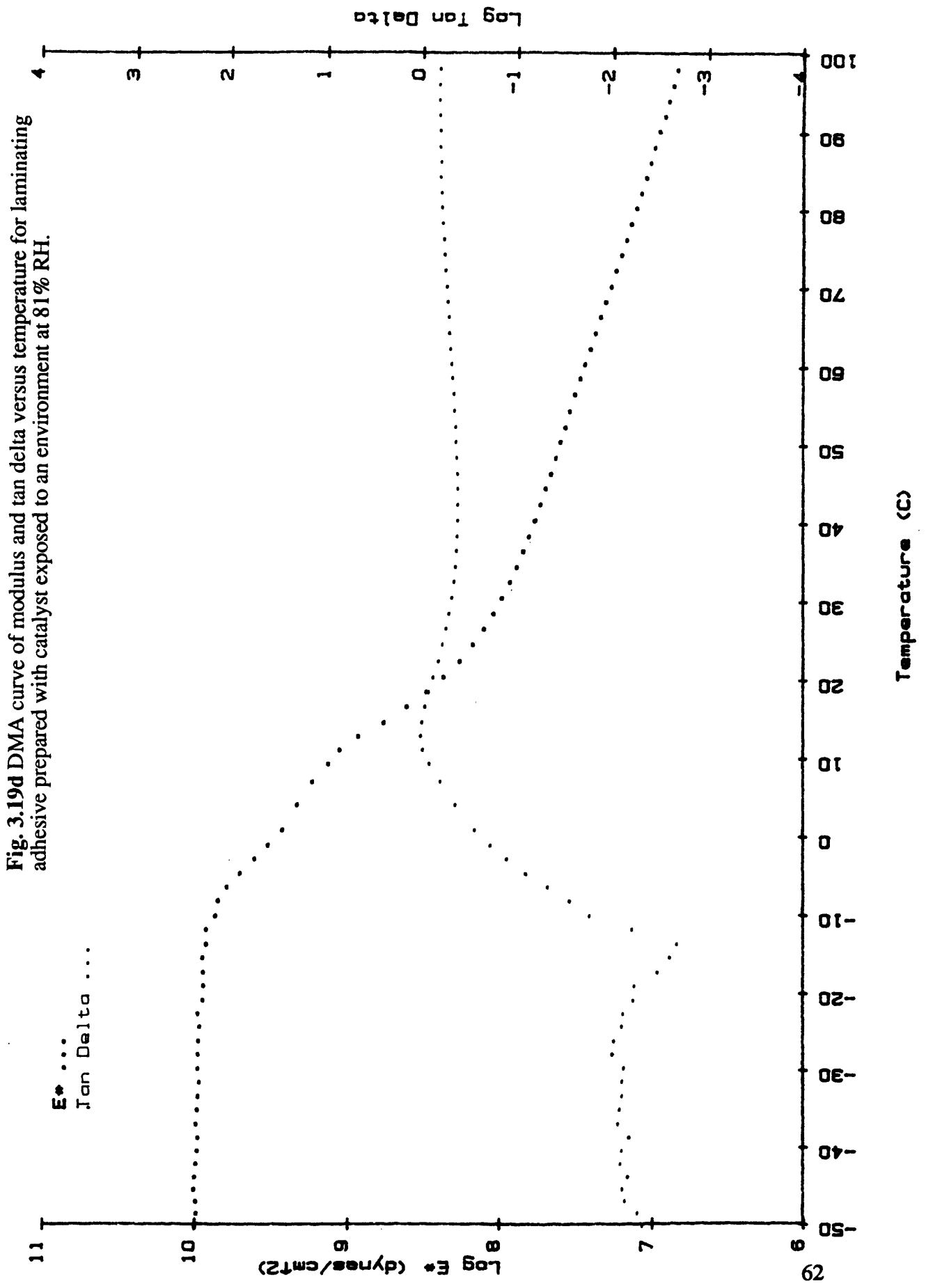

Fig. 3.19d DMA curve of modulus and tan delta versus temperature for laminating adhesive prepared with catalyst exposed to an environment at 81% RH.

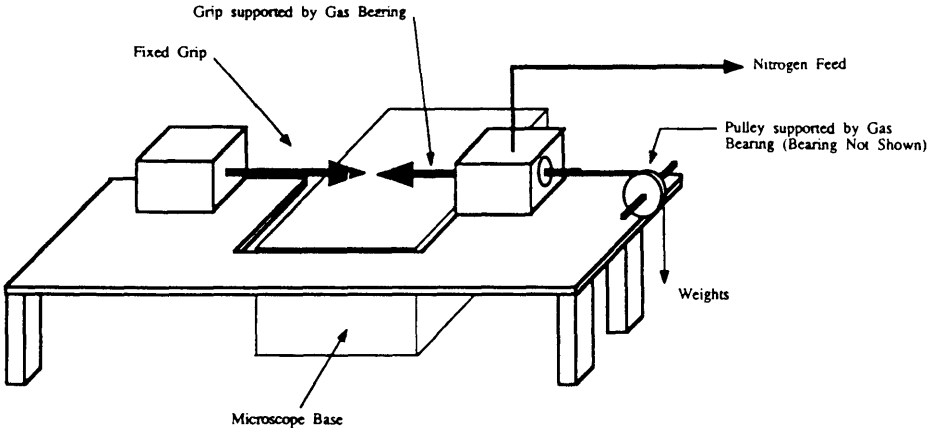

Fig. 3.20 Schematic diagram of device used for three point bend testing.

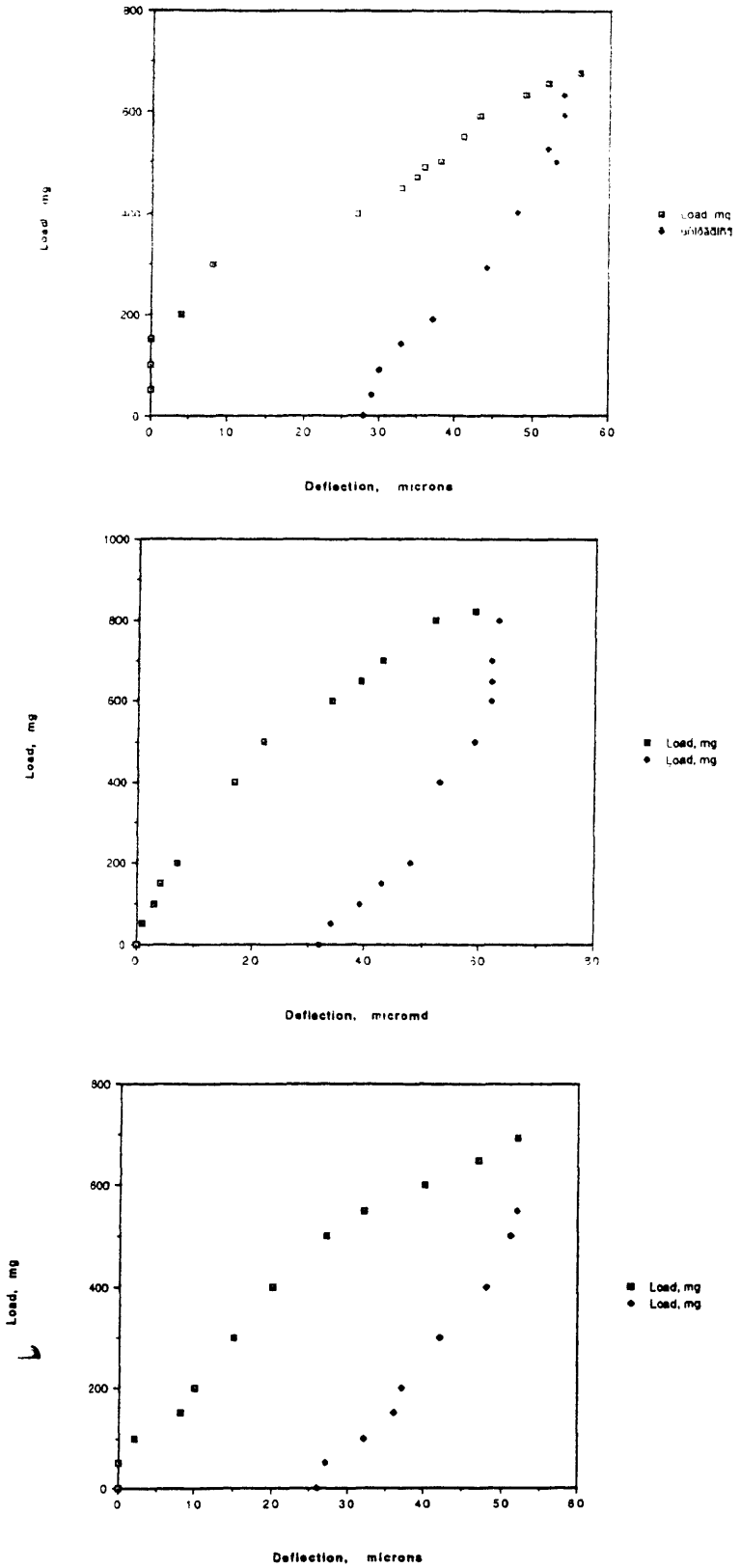

Fig. 3.21 Load versus deflection curves for three rail samples of Lot 7065. Both loading and unloading information is presented.

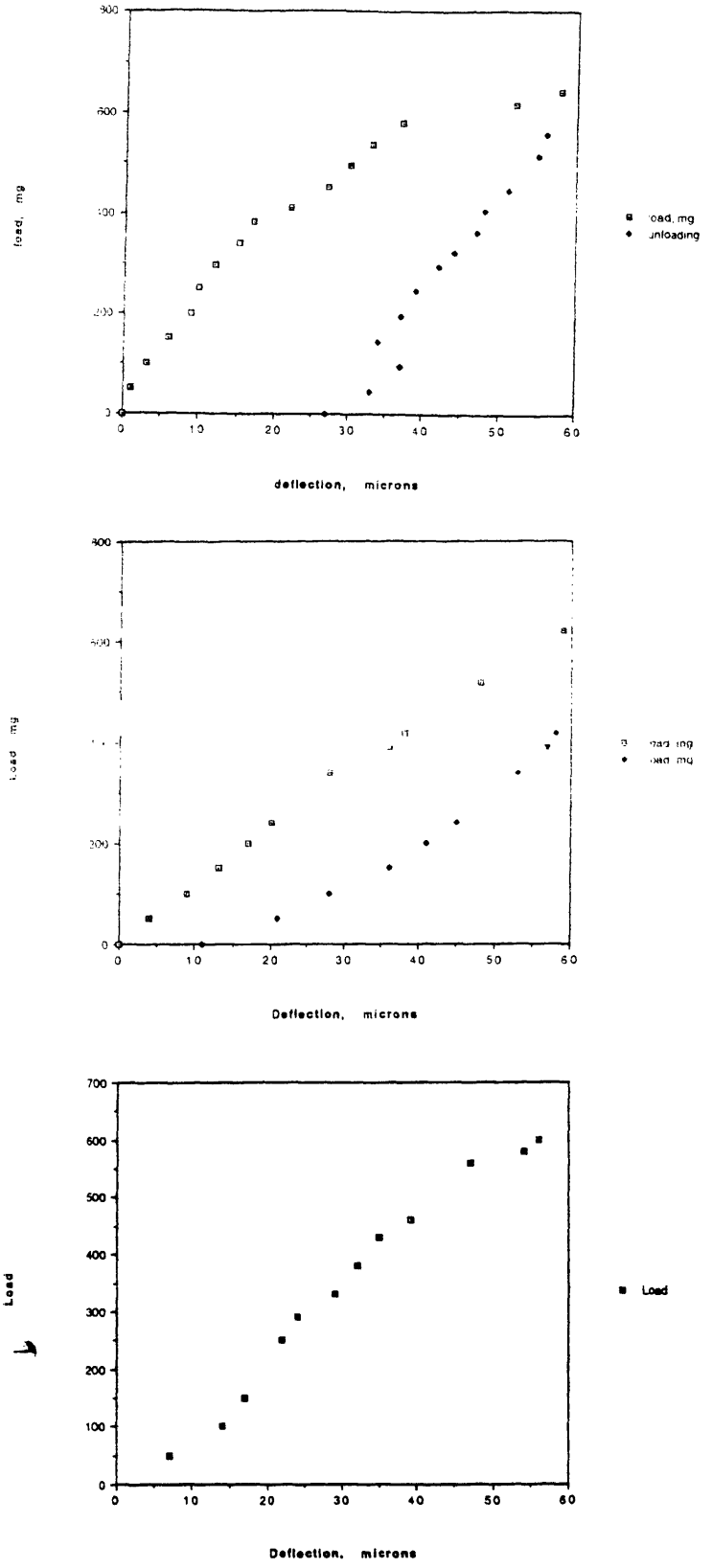

Fig. 3.22 Load versus deflection curves for three rail samples of lot 7084.

4. RAIL REDESIGN

The technical assessment of the standard seven layer laminate rail identified sources of material variability and provided a strategy for incremental improvement. However, it was concluded that the seven layer structure was intrinsically non-robust from a manufacturing stand-point and significant performance gains could not be easily achieved through a strategy of incremental improvement of the existing rail design. Instead, the project was redirected toward achieving a redesign of the standard rail which would more adequately fulfill the Captiva film product requirements. The goal of the redesign was a rail which would incorporate less intrinsic material variability and would be able to withstand higher stress levels during processing and thereby improve overall film yield.

4.1 Design Guidelines

The insights gained in the preliminary assessment of the standard rail led to the development of the following guidelines for the redesign to the rail component:

1. The total number of material sub-components should be reduced to eliminate processing defects at material interfaces.

2. Non-synthetic material sub-components, such as the tissue, should be replaced with synthetic and less variable materials or should be eliminated altogether.

3. The new rail should have a lower modulus, lower yield stress and higher toughness than the existing structure to enable more energy absorption before failure.

4. The new design must also fulfill all existing product requirements such as dimensional stability at assembly laminating temperatures, resistance to reagent, and compatibility with the negative and positive side heat seals.

4.2 Rail Redesign

Using the above guidelines, a three layer monobase rail design was developed. The design consists of a single polymer substrate film with one layer of heat seal applied to each side (see Fig. 4.1). A decision was made to incorporate the standard heat seals into the new design because of the complexity involved in developing other more mechanically stable heat seals which would be compatible with the positive and negative layers.

Fig. 4.1 Schematic of the standard seven layer rail design and three layer monobase redesign in cross-section.

The three layer or monobase redesign is seen as an improvement over the conventional seven-layer laminate in that it reduces the number of material interfaces from six to two and eliminates four material layers: two laminating adhesive layers and two tissue layers. The reduced number of converting operations required for the manufacture of the monobase redesign is another advantage.

4.3 Polymer Substrate Screening

Nine materials were initially identified as potential candidates for the substrate inner layer of the monobase design by fulfilling the following criteria:

1. resistance to alkali for compatibility with the developer
2. dimensional stability at 180 C (laminating temperature)
3. low modulus and high toughness relative to the current rail
4. availability in film form
5. resistance to MEK for compatibility with the heat seals

The candidates and selected material properties are listed below in Table 4.1. The commercial names of the candidate materials are not listed for proprietary reasons.

TEST LABEL	MODULUS PSI	Yld. Strength	% Elongation
Candidate 1	150,000	25,000	375-500
Candidate 2	330,000	6,500	150
Candidate 3	200,000	2,000	100
Candidate 4	100,000	12,300	300
Candidate 5	24,000	20,000	600
Candidate 6	53,000	5,300	350
Candidate 7	53,000	5,500	300
Candidate 8	230,000		
Candidate 9	360,000	12,000	180

Table 4.1 Polymer substrate candidates and selected material properties

The substrate candidates identified were put through a battery of bond measurements to determine their compatibility with the two heat seals and to determine if sufficient adhesion to the negative and positive sheets was possible. The bond testing was

done at Rexham Industrial by Tom Bezek and the results are listed in Table 4.2. The bond strengths are listed in grams.

NAME	GAUGE mils	NEGATIVE BOND gms	POSITIVE BOND grms
Candidate 1	2	500	120
Candidate 2 Dull side	3	40	500
		400 w/*P8* primer	
		40 with *4050* primer	
Candidate 2 Shiny side	3	40	700
		440 w/*P8* primer	
		40 with *4050* primer	
Candidate 3	3	760	120
Candidate 4	2	400	460
		300 w/*P8* primer	
		200 with *4050* primer	
Candidate 5	2	760	640
Candidate 6	4	200	200
Candidate 7	2	960	200
Candidate 8	2.5	500	600
		700 w/*P8* primer	
		500 with *4050* primer	
Candidate 9		1100-1200	1100-1200

Table 4.2 Polymer substrate bond values to negative and positive sheet .

On the basis of the measured bond strengths candidates 6 and 7 were eliminated from consideration. Bond strengths below 200 grams are considered unacceptable.

4.4 Production Trials

Production trials were successfully conducted with candidates 2, 3, and 9. A trial was attempted with candidate 1 but final frame assembly was unsuccessful because the knife on the assembly machine was unable to adequately cut the film. Trials were not conducted with the remaining candidate materials because of time constraints.

Film, incorporating monobase rails using candidates 2, 3, and 9 as substrates, was assembled and tested for leakage at 45°, 71° and 105° F. Leakage data for the film made with the experimental rails along with that for film made with a control lot of standard seven layer rail is presented in Fig. 4.2. For proprietary reasons the data are not presented in absolute terms. Fig. 4.2 presents the relative leakage levels of film made with the control rail and the monobase rails at three different temperatures.

The candidate 3 rail was clearly the poorest performer among the three candidates. At all three temperatures the candidate 3 rail contributed to significantly higher levels of leakage than did the control. The candidate 2 rail was comparable to the control at 71° and 105° but was significantly worse than the control at 45°.

Zero leakage was reported for the candidate 9 rail at all three temperatures. The most significant improvement over the performance of the control occurred at 45° at which the performance of the candidate 9 rail was clearly superior.

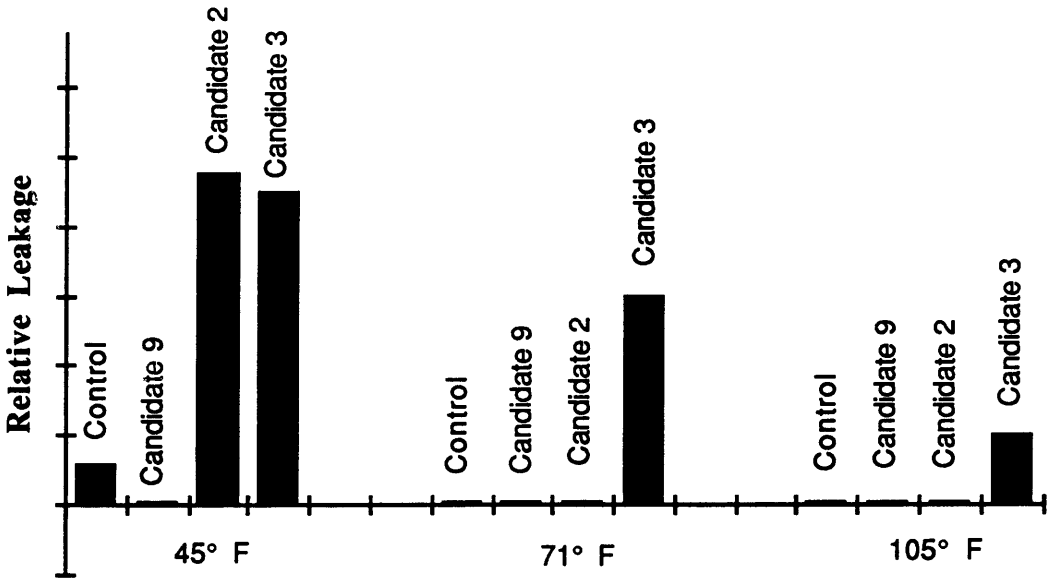

Fig. 4.2 Relative leakage at 45°, 71° and 105° F six days after assembly is presented for Captiva film made with one of four different rails: a control seven layer rail, and three monobase rails using either candidate 2, 3 or 9 as a substrate material. Zero leakage for the candidate 9 rail is reported at all three temperatures.

4.5 Conclusions

Based on preliminary production trials, the candidate 9 monobase rail is considered an attractive candidate for the replacement of the standard seven layer rail. Side seal leakage was virtually eliminated in test film made with the candidate 9 rail at the three standard testing temperatures. Currently, almost all production packs which are rejected on the basis of side seal leakage, are rejected because of leakage at 45°. This makes the low temperature performance advantage of the candidate 9 material especially significant. The improved performance of the candidate 9 rail can potentially translate into an estimated $2.5M annual savings. The candidate 9 rail is being strongly considered as a replacement for the standard seven layer rail and more extensive production trials and temperature and humidity cycling tests are currently scheduled.

Another advantage of the candidate 9 three layer rail is its potential to be a less expensive component than the standard seven layer rail because of reduced material and manufacturing costs. The candidate 9 rail eliminates tissue and adhesive layers and its

three layer design requires fewer converting operations. The monobase rail also has the potential to be a much less variable component because of the reduced number of interfaces and better material uniformity of the candidate 9 material .

Modulus and toughness were both considered significant mechanical parameters in determining the performance of the Captiva side seal. However, an accurate prediction of rail performance was not made on the basis of mechanical properties alone. Modulus versus toughness values for the monobase substrate candidates as well as standard rail and straight polyester sheet are presented in Fig. 4.3. Toughness was calculated as area under the stress/strain curve to the point of failure and is reported as Energy at Break in units of lbs-in. Modulus was calculated in psi and is reported in thousands of psi.

There is a broad correlation apparent in Fig. 4.3, between low leakage levels and low modulus and high toughness relative to the performance of the standard rail. However, a trend is not clear between the candidate 2, 3, and 9 materials. Factors which affect adhesion, such as surface roughness and contact angle, may provide further insight into the performance of the different materials and are discussed in Chapter Five.

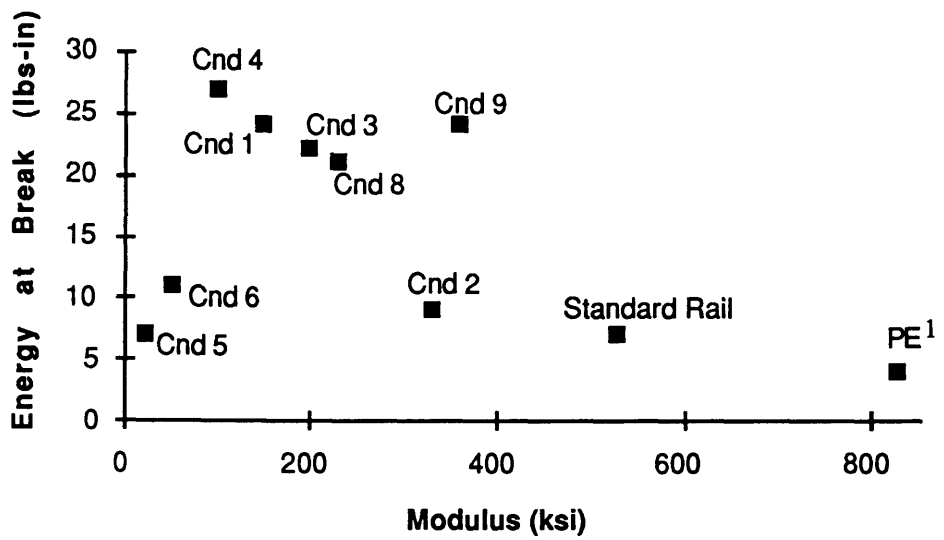

Fig. 4.3 Modulus versus Energy at Break (toughness) for the substrate candidates along with a representative value for the standard seven layer rail structure. [1] PE designates the polyester core material used in the standard rail.

5. NEW RAIL CHARACTERIZATION

The development of relevant supplier specifications for key material components is considered crucial for the support of robust, high quality manufacturing processes. If relevant material properties for product performance and their acceptable ranges are not well established, key parameters may shift undetected and affect manufacturing processes adversely. It is not uncommon for a material supplier to provide the same product to several customers, each of which may have vastly different applications for the material and correspondingly different requirements. A material parameter may be changed slightly to accommodate one customer or the supplier itself, causing problems for other customers, who without a thorough understanding of their key parameters may not be able to identify the cause of the change in their process.

The work documented in this chapter is an effort to lay the foundation for developing relevant material specifications for the Captiva rail redesign by characterizing a lot of high level performing candidate 9 material. The fact that different lots of standard rail, having met all supplier specifications, varied widely in performance for no identifiable reason indicated that all the key variables in the Captiva side seal system were not understood. Several material properties, such as wetting angle and surface roughness, are presented in this chapter in an attempt to document other parameters that might be factors in determining rail performance. Conclusions are not drawn as to whether or not the material properties studied have a significant impact on rail performance. Rather, the data are presented as an aid for correlating rail properties and performance when sufficient production and test data are available which in turn will enable the development of relevant supplier specifications for the three layer Candidate 9 material based rail.

5.1 SEM Cross - Sections

The candidate 9 material is a blend of two incompatible polymers. When the two materials are mixed initially, the polymer that is added in the lowest percentage forms small voids where it pulls away from the other polymer matrix (see Fig. 5.1). As the blend is processed and heated, the inner surfaces of the voids in the matrix become coated with the other polymer. Later, as the material is formed into a film, the circular voids in the matrix take on an elongated shape.

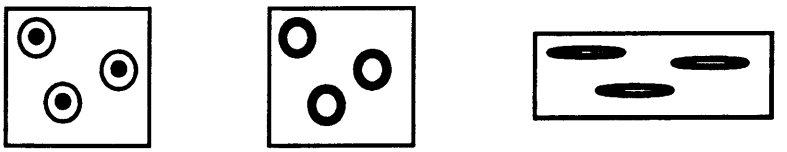

Fig. 5.1 A schematic of the candidate 9 material morphology at different stages in its forming process. (A) After initial mixing voids are formed where one polymer pulls away from the other (B) When heated the inner surfaces of the voids become coated (C) During final film forming the voids become elongated.

The elongated voids are visible in SEM cross-sections taken of the candidate 9 material (see Fig. 5.2). The voids are approximately 10 microns in length. The quantity and size of the voids potentially may have a significant impact on the ability of the material to absorb energy during deformation. The sample preparation procedure used for taking SEM micrographs of the candidate 9 material is described in sections 3.1 and 3.2.

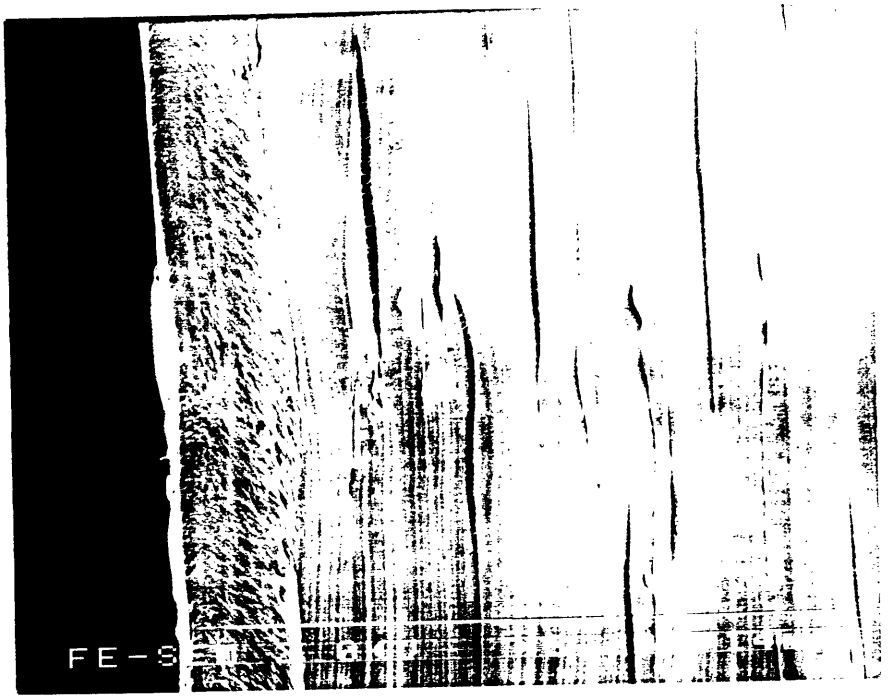

Fig. 5.2 SEM micrograph of the candidate 9 material in cross-section. Elongated voids are visible.

5.2 Surface Roughness

Surface roughness measurements were taken of candidate 9 film samples using a WYKO Roughness/Step Tester with a 10x objective. Surface roughness was studied because of its potential impact on adhesion. The WYKO tester is a vertically scanning interference microscope system. The microscope objective contains an interferometer which consists of a reference mirror and beam splitter that produce interference fringes when light reflected off the reference mirror combines with light reflected off the sample. The RST uses a standard microscope lamp emitting short-coherence length white light as light source so interference fringes are only present over a very shallow depth on sample

surfaces. Samples are profiled by scanning vertically so that each point on the surface produces an interference signal.

The RST starts a measurement sequence by focusing above the top of the surface being profiled and quickly scanning downward. At evenly spaced intervals during the scan, frames of interference data imaged by the video camera are captured and processed. As the system scans downward, an interference signal for each point on the surface is formed. The system uses a series of computer algorithms to precisely locate the peak of the interference signal for each point on the surface.

Two surface roughness measurements were taken of each side of a sample candidate 9 film which was used in the production trials of the monobase rails, the results of which are summarized in section 4.4. This work was done under the direction of Saroj Roy. Average roughness (Ra), root mean squared roughness (Rq), maximum peak to valley height (Rt) are presented for the four areas tested in Table 5.1 along with values for Q value and Q percent. Q value is a modification of the standard peak-to-valley difference, the difference between the highest and the lowest point in the data set. However, Q value differs in that it eliminates the data values outside of the Q percent, which tend to be infrequently occurring heights. If the Q percent is set to 99% the Q value is calculated without the extreme 1% of data points. The Q value may depict the overall surface figure more realistically than the standard Rt by not considering extreme data points which may represent surface contaminants. The inner surface of the material roll is referred to as Side B and the outer surface as Side A.

	Average Roughness	RMS Roughness	Max. Peak to Valley Height	Q Percent	Q Value
Side A #1	802.37 nm	1.180 um	11.585 um	99.05	6.243 um
Side A #2	884.497 nm	1.311 um	9.542 um	99.01	7.241 um
Side B #1	172.956 nm	226.935 nm	3.651 um	99.09	1.164 um
Side B #2	181.863 nm	274.858 nm	6.040 um	99.04	1.178 um

Table 5.1 Surface Roughness Parameters

Two types of plots for each surface were generated; a two-dimensional surface profile and a surface histogram at Q percent set to 99 and are presented in Figs 5.3 - 5.10. Each histogram of surface values indicates how often various heights occur in the data. Surface histograms are useful because they "filter-out" a percentage of the highest peaks and lowest valleys effectively smoothing the data of the inadvertent presence of dirt or contaminants.

5.3 Contact Angle

The contact angle of a standard liquid on a materials surface characterizes surface energy and affinity for bonding which has an effect on the adhesive properties of the material. For that reason, the contact angle of water was measured along various spots across the length of a strip of candidate 9 film. An average of five to eight measurements were taken from which an average was calculated. The average value for contact angle of side A was 78° with a range from 75° to 80° and the average for side B was 101° with a range from 100° to 104°. The measurements were done under the supervision of Saroj Roy.

5.4 Conclusions

Mechanical property information alone was shown to be insufficient in explaining the improved performance of the three layer candidate 9 based rail. The work presented in this chapter is the first step in laying the foundation for determining what other material parameters significantly effect rail performance. To ensure a robust, high quality Captiva manufacturing process, rail properties and performance must be correlated as sufficient production and test data become available. Without such a base of information, relevant supplier specifications cannot be developed.

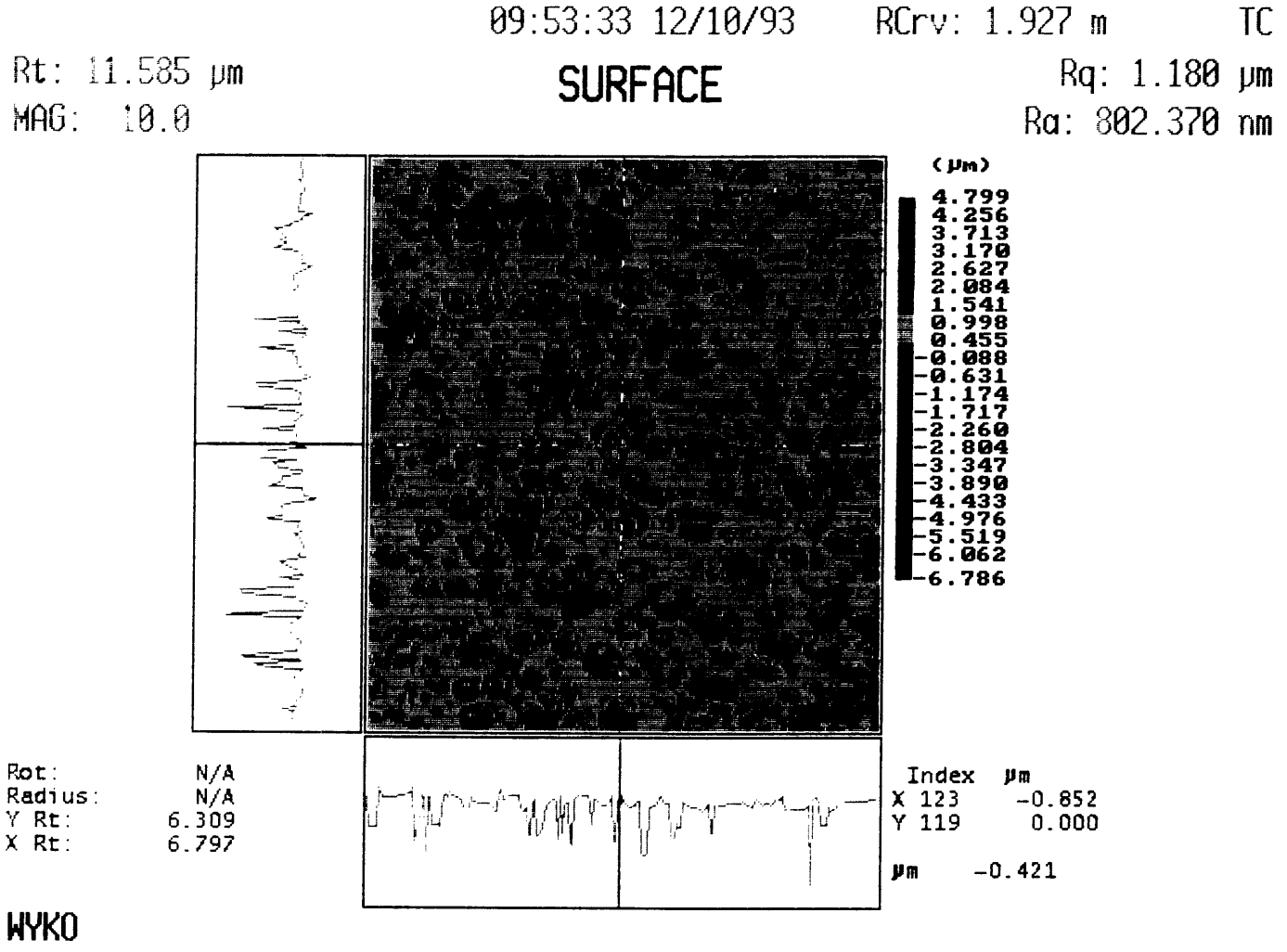

Fig. 5.3 Surface profile of a candidate 9 film sample. The outer surface of the material roll was analyzed and is designated Side A #1. Average roughness and RMS roughness are reported as 802.37 nm and 1.180 um respectively.

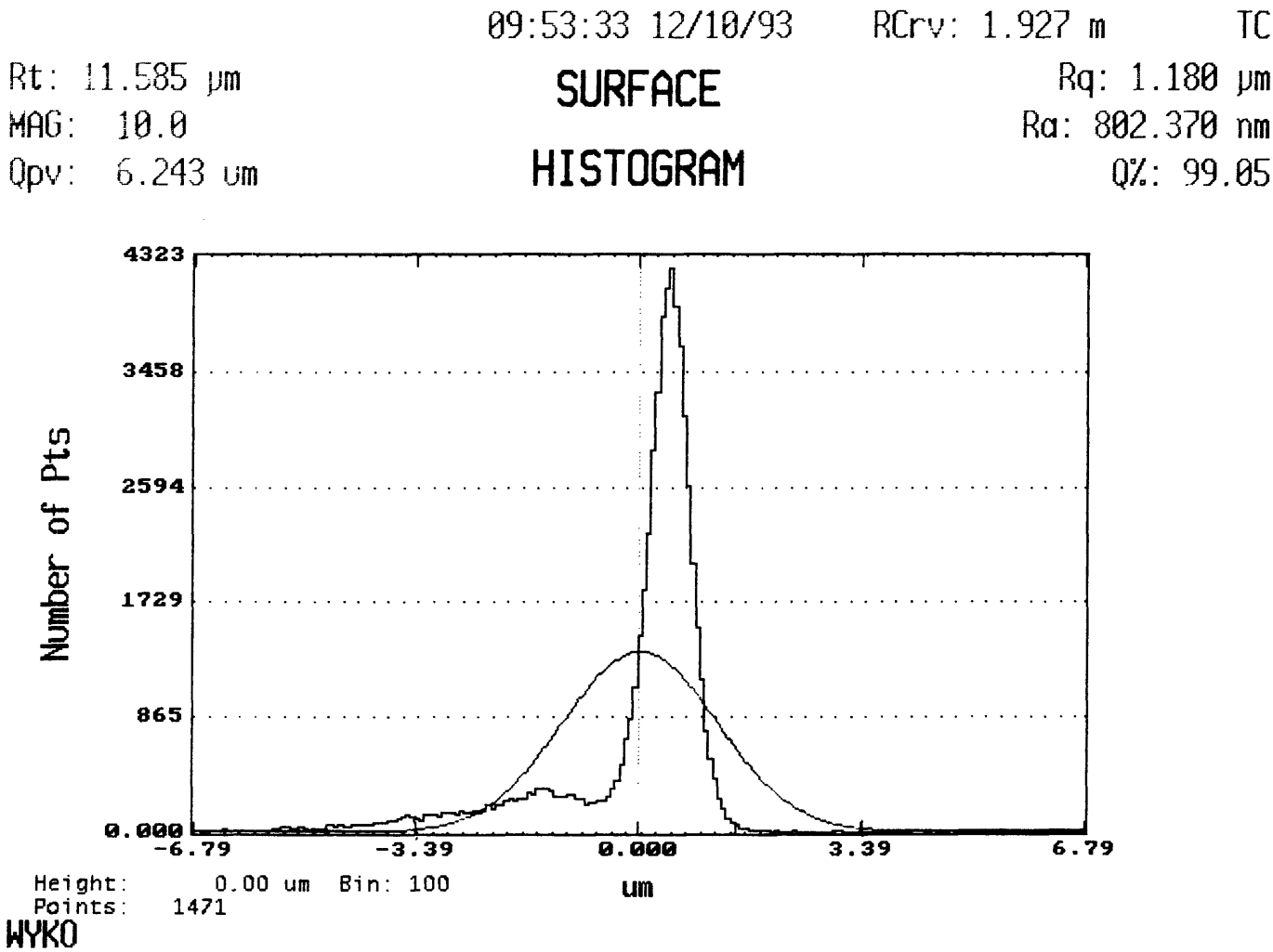

Fig. 5.4 Surface histogram of a candidate 9 film sample. The outer surface of the material roll was analyzed and is designated Side A #1. Q percent was set to 99.05 and Q value was calculated as 6.243 um. Max. peak to value height is reported as 11.585 um.

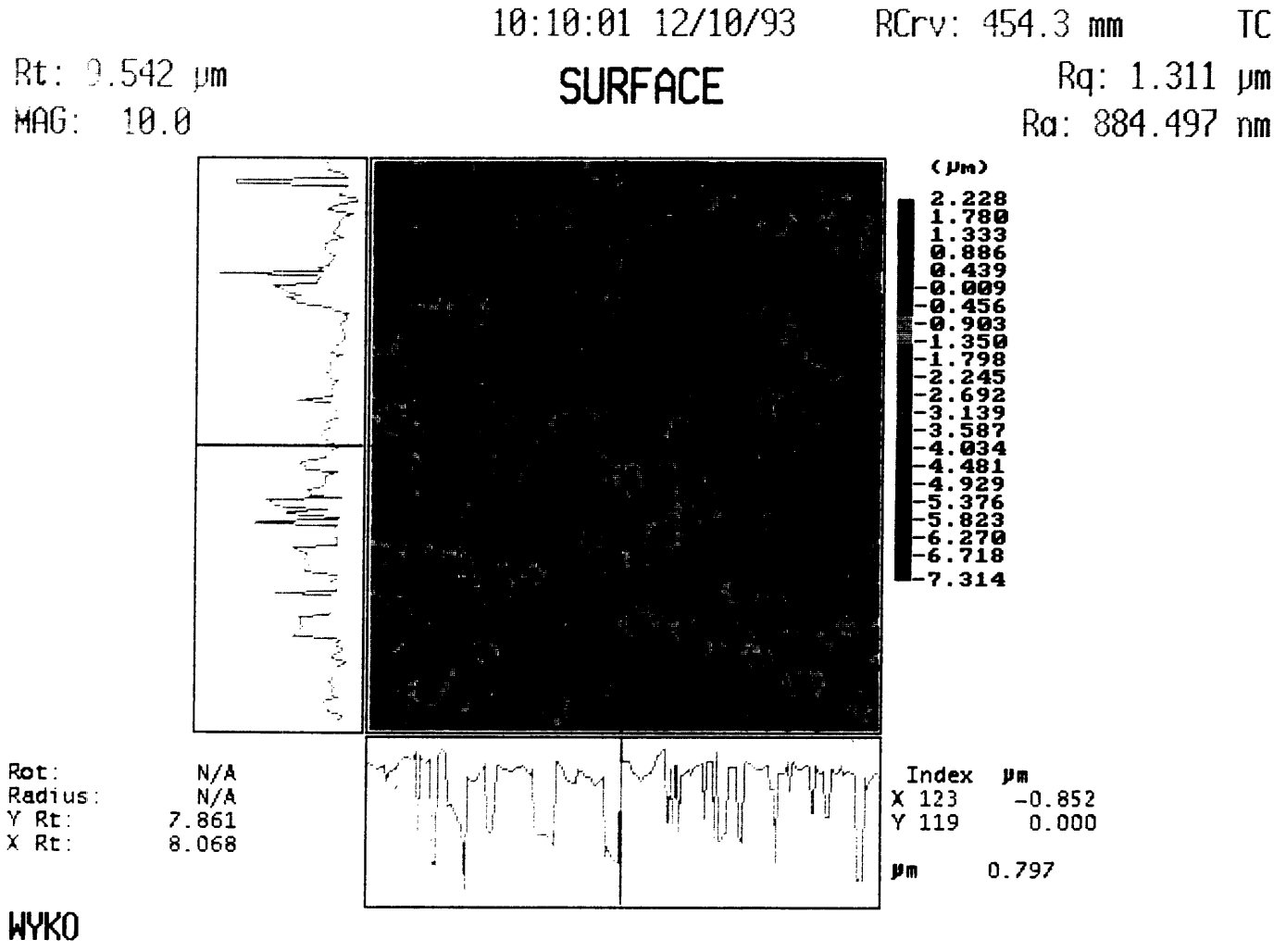

Fig. 5.5 Surface profile of a candidate 9 film sample. The outer surface of the material roll was analyzed and is designated Side A #2. Average roughness and RMS roughness are reported as 884.497 nm and 1.311 um respectively.

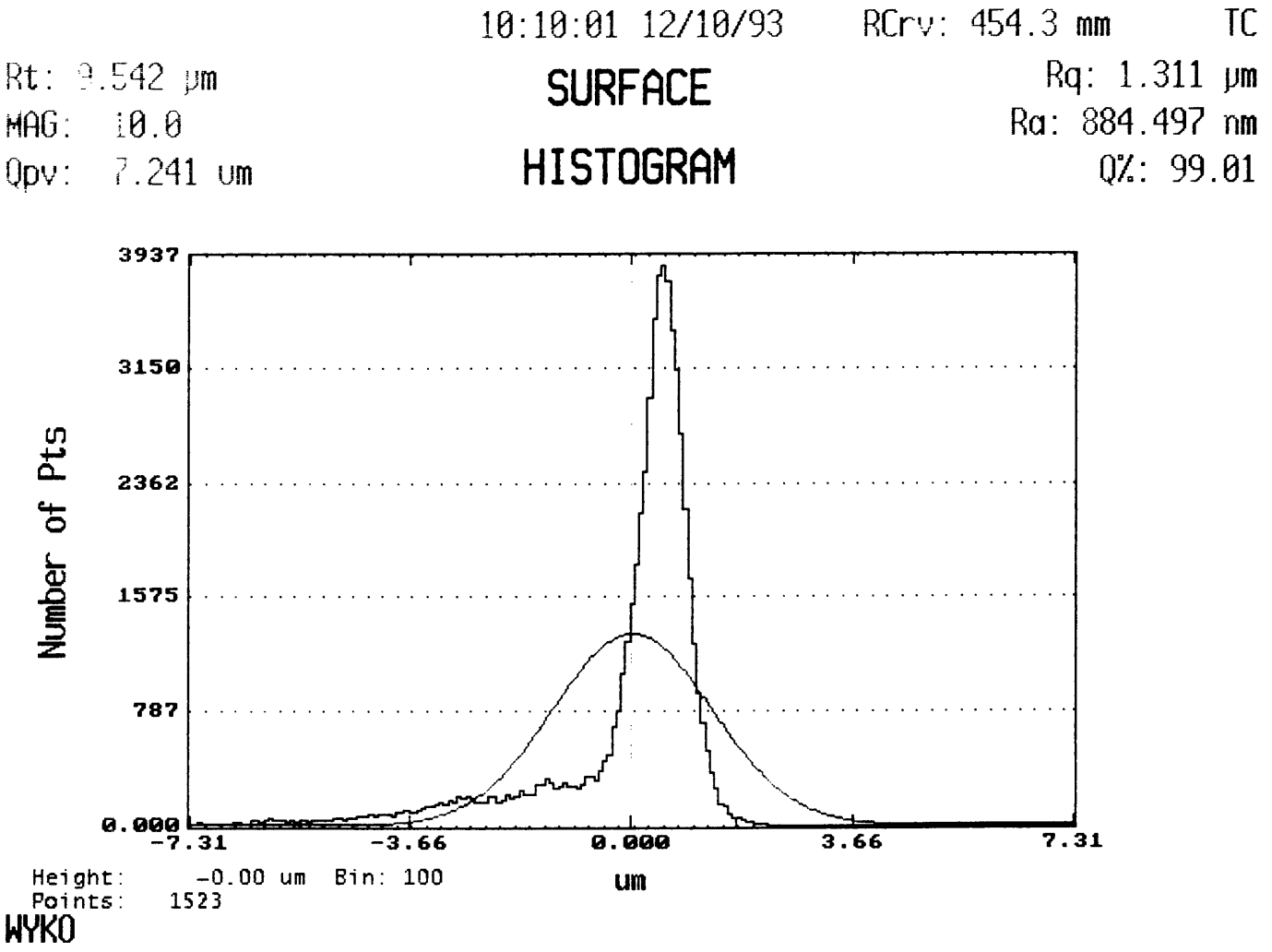

Fig. 5.6 Surface histogram of a candidate 9 film sample. The outer surface of the material roll was analyzed and is designated Side A #2. Q percent was set to 99.01 and Q value was calculated as 7.241 um. Max. peak to value height is reported as 9.542 um.

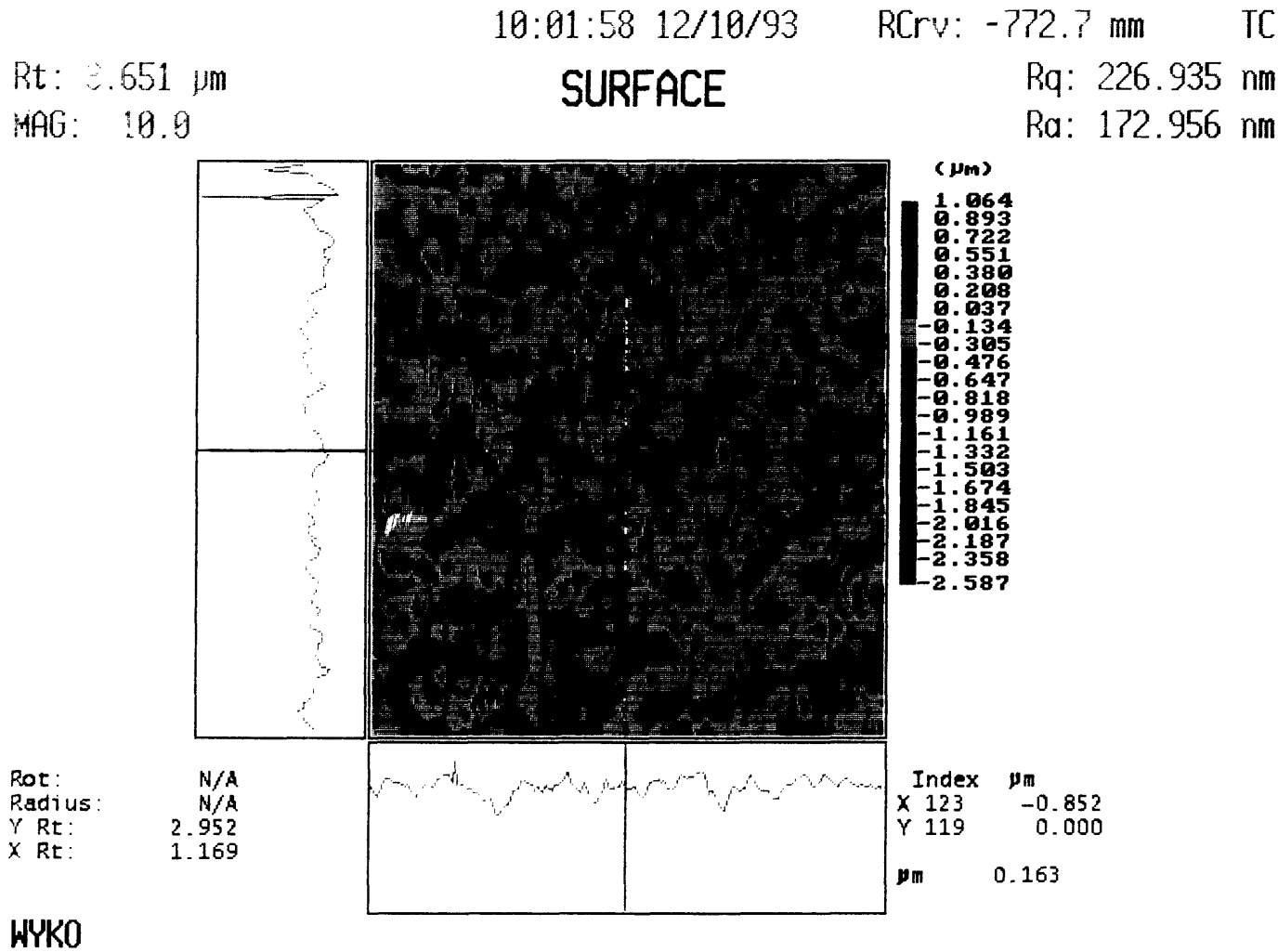

Fig. 5.7 Surface profile of a candidate 9 film sample. The inner surface of the material roll was analyzed and is designated Side B #1. Average roughness and RMS roughness are reported as 172.956 nm and 226.935 nm respectively.

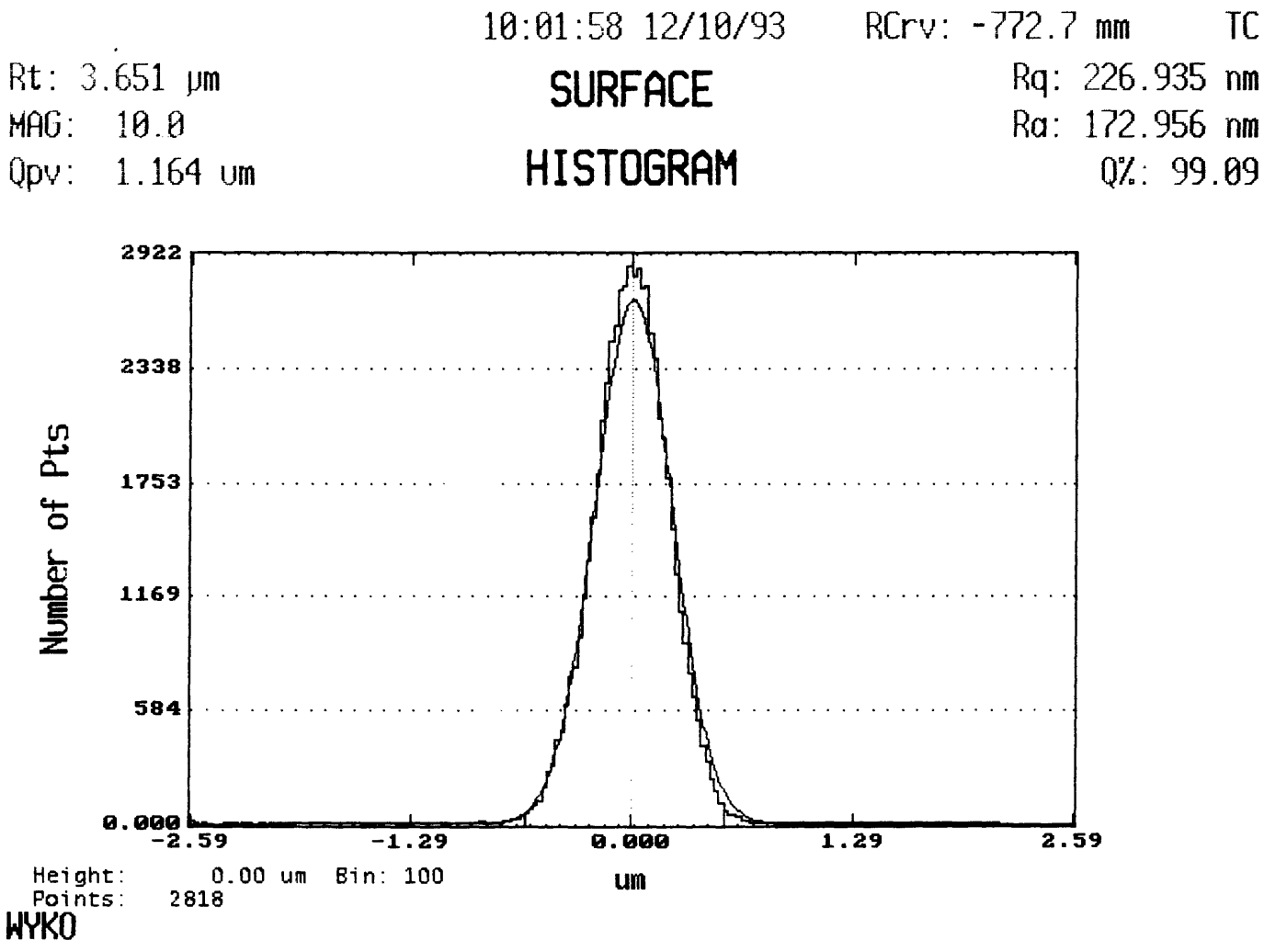

Fig. 5.8 Surface histogram of a candidate 9 film sample. The inner surface of the material roll was analyzed and is designated Side B #1. Q percent was set to 99.09 and Q value was calculated as 1.164 um. Max. peak to value height is reported as 3.651 um.

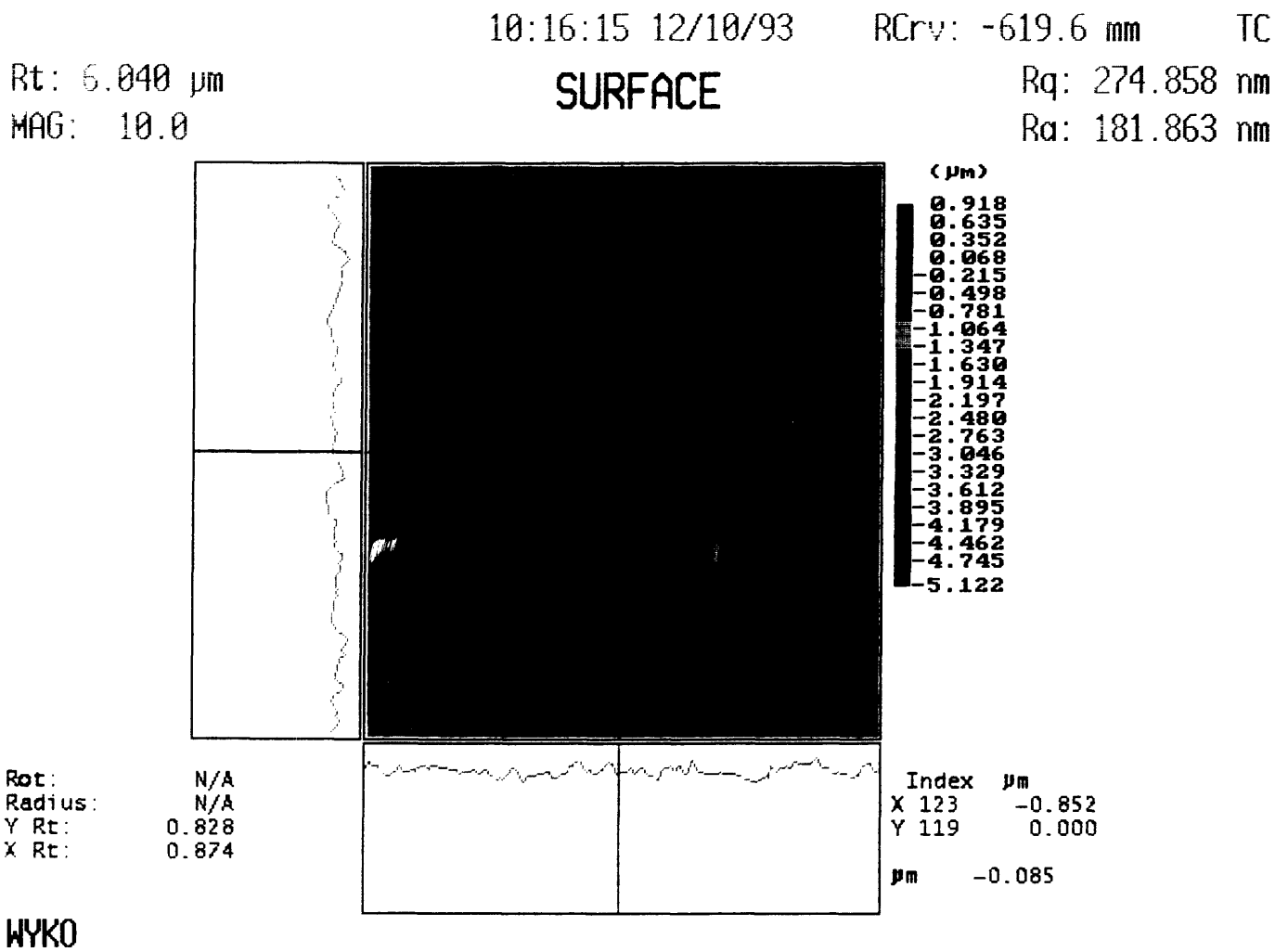

Fig. 5.9 Surface profile of a candidate 9 film sample. The inner surface of the material roll was analyzed and is designated Side B #2. Average roughness and RMS roughness are reported as 181.863 nm and 274.858 nm respectively.

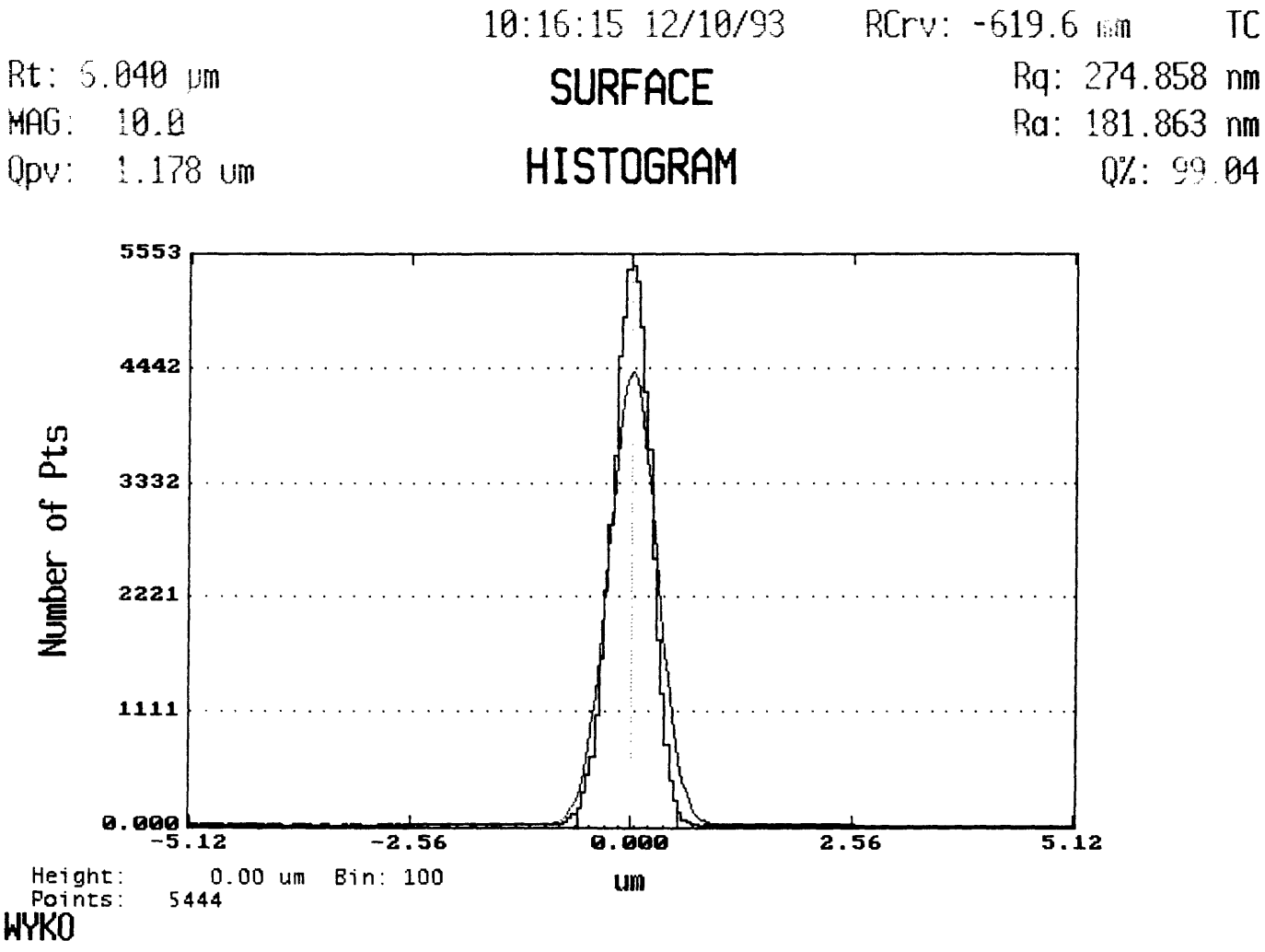

Fig. 5.10 Surface histogram of a candidate 9 film sample. The inner surface of the material roll was analyzed and is designated Side B #2. Q percent was set to 99.04 and Q value was calculated as 1.178 um. Max. peak to value height is reported as 6.040 um.

6. CONCLUSIONS AND RECOMMENDATIONS

The Captiva rail redesign project reflects the cumulative efforts of many individuals from organizations across Polaroid, Polaroid suppliers and MIT. The project provides an example of the technical and bottom line improvements that can be achieved by effectively coordinating the appropriate resources with a clear and coherent project strategy. Many of the project's contributions can be attributed to the utilization of key technical resources outside the manufacturing organization and a project strategy aimed toward improving manufacturing robustness.

6.1 Research and Development's Role in Manufacturing Support

Polaroid's Research and Development organization consists of top-notch technical personnel and outstanding analytical resources which are not frequently utilized for the support of on-going manufacturing operations. Over the course of the rail project, key individuals in the R&D organization were brought in as internal consultants through informal means. Individuals with expertise in areas relevant to the rail project were identified through word of mouth and their time spent on the project was outside of their official responsibilities. They were invaluable in providing technical expertise in the fields of polymer mechanics and adhesion and contributed to the definition of the project strategy. Benefits from that contact with the R&D individuals goes beyond contributions made to the rail project. Many of the analytical techniques and much of the engineering theory that they introduced to the team can be applied to future manufacturing problems.

To encourage the type of cross-functional collaboration that occurred on the rail project, Polaroid should create a mechanism for recognizing and rewarding individuals'

contributions to projects that benefit the company as a whole but are not part of their official responsibilities and facilitate the identification of individuals throughout the company who might act as technical resources by creating a directory listing people and their areas of technical expertise. As a company Polaroid can realize significant gains by tapping into resources that traditionally focus on new product development to support existing production without adversely affecting the performance of its R&D organization.

6.2 Redesign for Manufacturing Robustness

The strategy of redesigning the rail component to achieve manufacturing robustness proved to be very effective. By working toward a rail design whose performance was inherently less sensitive to input parameters, not only were the desired gains in film yield achieved, but a reduction in material and sub-component assembly costs were also realized. Many other integral film components are as complex or more complex than the standard seven layer rail (see Fig. 2.1). It is likely that the proactive reevaluation and redesign of other integral film components using the strategy that was outlined in this thesis would lead to gains similar to those achieved by the monobase rail redesign.

References

McGarry, F.J. and J.E. Moalli. *Mechanical Behaviour of Rigid Rod Polymer Fibres: Measurement of Axial Compressive and Transverse Tensile Properties*. Polymer. Vol. 32, No. 10, 1991.

Murayama, T. Dynamic Mechanical Analysis of Polymeric Materials. New York: Elsevier Scientific Publishing, 1978.

Timoshenko, Stephen and James Gere. Mechanics of Materials. Monterey,California: Litton Educational Publishing, Inc. 1972.

Ward, I.M. Mechanical Properties of Solid Polymers. New York: Wiley, 1983.